Chapter 10

Fluorescent nanodiamonds

Anna Ermakova[1,2]

[1]*Royal Belgian Institute for Space Aeronomy, Brussels, Belgium,* [2]*Institute for Materials Research, Hasselt University, Hasselt, Belgium*

10.1 Introduction

The fluorescent properties of nanodiamonds can be related to either the presence of amorphous sp^2 carbon on the surface or optically active crystal defects—color centers. The fluorescence nature is connected to the fabrication methods of nanodiamonds and their postprocessing (irradiation, annealing, and surface treatment). Nanodiamonds with optically stable color centers have broad potential applications in different directions of quantum technology, from imaging and sensing to communication and computing. The significant advantage of diamond color centers is that their emission properties are independent of the nanocrystal size in contrast to quantum dots, for instance (Alivisatos, 1996; Smith et al., 2009). However, they are sensitive to the surrounding crystal defects that also include a surface and its chemical functionalization. In the case of the bulk diamond, it is possible to localize color centers deep enough into the crystal volume to reduce the surface influence; however, for nanodiamonds, especially ultrasmall ones, and various fabricated diamond-based photonic structures, the surface plays a significant role that can not be ignored. Its impact can be controlled and sometimes reduced by different chemical treatments and functionalizations; nevertheless, it cannot be mitigated completely. Therefore, the charge and optical properties of color centers placed close to the diamond surface depend on the chemical groups on it. The knowledge obtained from the nanodiamond surface treatment can significantly impact the understanding of the practical creation of photonic systems fabricated not necessarily with nanodiamonds but also from bulk diamond crystals.

10.2 Production of nanodiamonds

The fabrication of nanodiamonds can be done using a few techniques that influence the properties of obtained samples. Generally, the production methods can be divided into bottom-up and top-down synthesis. The bottom-up approach is based on nanodiamond synthesis from carbon-containing materials such as graphite, adamantane, or protein-like chains. Such a strategy of moving from a single molecule level to a crystal-structured material includes the following methods: detonation synthesis, chemical-vapor deposition (CVD), and high-pressure high-temperature synthesis (HPHT). Depending on the synthesis method to grow a diamond crystal, different conditions, such as temperature and pressure, are needed (Fig. 10.1). However, nanodiamonds can also be produced by milling a bulk diamond crystal into nanocrystals. Natural or synthetic (CVD or HPHT) diamonds can be used as a starting material for this top-down method. Each fabrication process delivers nanodiamonds with various characteristics, such as size and shape distridutions or impurities, which are predefined by the synthesis approach. Postsynthesis treatments are based on the initial sample state and final requirements. For instance, they involve creating color centers through irradiation and/or activating them by annealing or surface cleaning and protection, which are determined by the final application.

10.2.1 Nanodiamonds in nature

Diamonds, in general, are not exotic materials; there are diamond mines on different continents. Therefore, some big or fancy-colored natural diamonds appear occasionally in the news. Probably everyone knows that they can be found in specific areas—volcanic pipes. However, large natural diamond crystals are still scarce, and their cost increases dramatically with the size. Such natural diamonds result from long-time high-pressure annealing of kimberlite, an igneous rock. The natural process of diamond formation is similar to the HPHT method uesd in laboratories. However, due to the

Nanophotonics with Diamond and Silicon Carbide for Quantum Technologies. DOI: https://doi.org/10.1016/B978-0-443-13717-4.00010-4

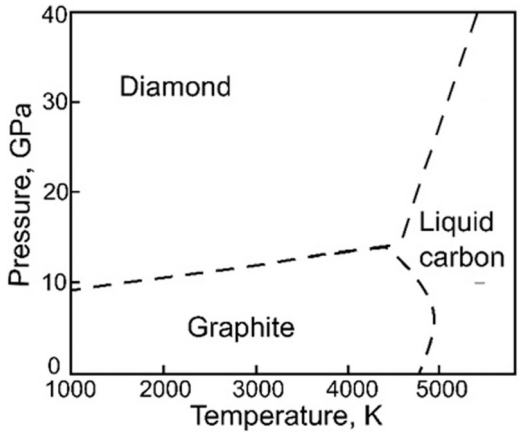

FIGURE 10.1 Carbon phase diagram. Phase diagram of the equilibrium between diamond, graphite, and liquid carbon.

extremely long annealing time inside the Earth, the crystal defects inside natural and synthetic HPHT diamonds and moreover CVD are significantly different (Mainwood, 1999). Since we talk about nanodiamonds here, the reasonable first question is, where can we find them in nature? The answer is fascinating. The highest number of natural nanodiamonds can be found in space (Greaves et al., 2018; Kinzie et al., 2014; Vlasov et al., 2014). They are created as the result of exposures during space evolution. Thus, discovered natural nanodiamonds are made by the detonation-like method in space. The nanodiamonds spinning around stars are considered to be a source of anomalous microwave emission, with brightness peaks at tens-of-gigahertz frequencies (Greaves et al., 2018). The presence of natural nanodiamonds on Earth is a powerful source of information about the Earth's evolution (Kinzie et al., 2014).

10.2.2 Detonation nanodiamonds

The first production of detonation nanodiamonds were realized by K.V. Volkov, V. Danilenko, and V.I. Elins in 1960–1965 (Danilenko, 2004). During the first experiments, nanodiamonds were obtained by shock compression of graphite and carbon black. The use of a graphite–metallic coolant mixture in this process allowed an increase in the yield by an order of magnitude. At the same time, these scientists synthesized nanodiamonds through an explosion of boron nitride and, later, of carbon molecules. A schematic presentation of the formation of detonation nanodiamonds is shown in Fig. 10.2 (Mochalin et al., 2012).

Detonation nanodiamonds are characterized by extremely small sizes, down to a single nanometer in diameter (Baitinger et al., 2012; Mochalin et al., 2012). However, these dimensions correspond to actual crystal-structured cores (Fig. 10.3). In reality, the structure of detonation nanodiamonds combines two types of carbon: crystal-structured sp^3 carbon of ultra-small cores and amorphic sp^2 carbon around them. As a result, detonation nanodiamonds are mainly clusters of a few ultracrystal cores in the matrix of the amorphic carbon with a total size of 10 nm and bigger (Fig. 10.3) (Baitinger et al., 2012). The ratio of sp^2 to sp^3 carbon in detonation nanodiamonds is related to the initial material used for the production and postproduction treatment. For example, it was shown by Reineck et al. (2017) that depending on a postfabrication treatment of obtained material, the final presence of sp^2 carbon could vary from 30 % for hydrogenated detonation nanodiamonds to 6 % for carboxylate one; for more details, see Table 10.1.

10.2.3 Chemical-vapor deposition nanodiamonds

Another bottom-up method to produce nanodiamonds is chemical vapor deposition. In this case, a diamond structure is formed from carbon-containing gases, particularly methane molecules CH_4 (Pruski et al., 1994). This technique recommends itself well for growing ultrapure bulk diamonds with minimal parasitic defects related to unwanted impurities or structural defects. The nanodiamond growth can be done on different types of substrates, such as silicon, copper, chromium layer, etc. (Fig. 10.4A) (Degutis et al., 2016; Gottlieb et al., 2016; Shershulin et al., 2015). Also, ultrasmall nanodiamonds can be used to initiate and determine the position of CVD-grown nanodiamonds, for example, detonation one (Degutis et al., 2016).

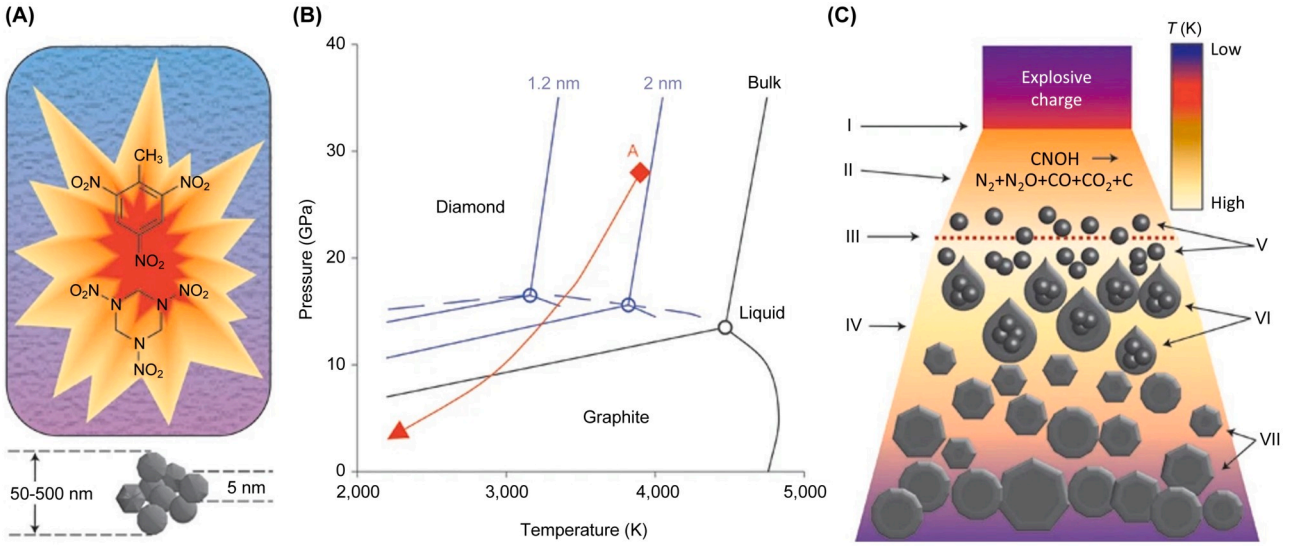

FIGURE 10.2 Typical scheme of detonation synthesis of nanodiamonds. (A) Explosion of a mixture of 60 % trinitrotoluene $C_6H_2(NO_2)_3CH_3$ and 40 % hexogen $C_3H_6N_6O_6$ and (B) its representation on the phase diagram. (C) Schematic of the detonation wave propagation showing different steps. All images are from Mochalin et al. (2012).
Source: From Mochalin, V. N., Shenderova, O., Ho, D., & Gogotsi, Y. (2012). The properties and applications of nanodiamonds. *Nature Nanotechnology*, *7*(1), 11–23. https://doi.org/10.1038/nnano.2011.209.

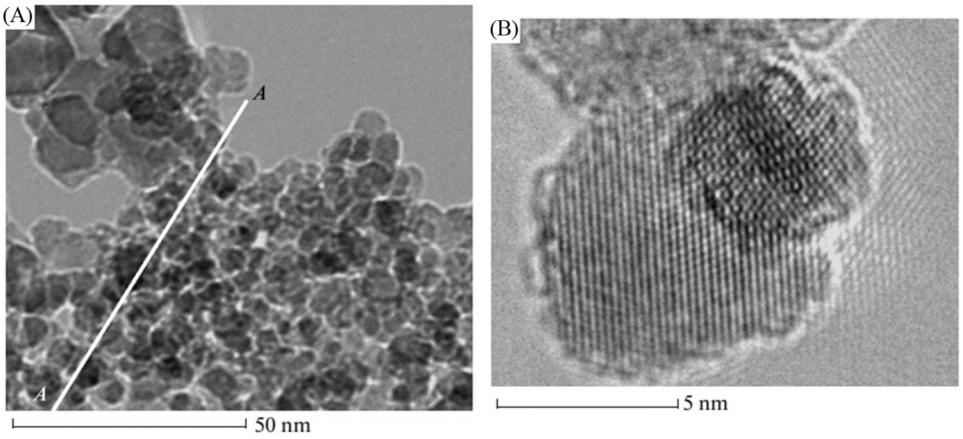

FIGURE 10.3 Transmission electron microscopy of detonation nanodiamonds. (A) Transmission electron microscope image of a detonation nanodiamond powder. (B) A high-resolution transmission electron microscope image of selected nanodiamonds. All images are from Baitinger et al. (2012).
Source: From Baitinger, E. M., Belenkov, E. A., Brzhezinskaya, M. M., & Greshnyakov, V. A. (2012). Specific features of the structure of detonation nanodiamonds from results of electron microscopy investigations. *Physics of the Solid State*, *54*(8), 1715–1722. https://doi.org/10.1134/s1063783412080057.

The advantage of CVD nanodiamond formation is that it allows crystal doping with the selected type of atoms with minimum parasitic defects compared to implantation doping, where a lot of radiation defects are created. It is especially crucial for doping with big atoms such as silicon or germanium. Until now, the best-observed properties of silicon-vacancy (SiV) centers in nanodiamonds in the case of line width were exactly for CVD-produced samples (Li et al., 2016). Nanodiamond formation with the CVD method allows control of the size of nanocrystals by variation of the growing time (Shershulin et al., 2015).

An additional positive opportunity provided by the CVD technique is the possibility of synthesizing more complicated structures on nanodiamonds. Firstly, nanodiamonds with different color centers can be fabricated. Moreover, chosen defects can be localized in separate overgrown layers of nanocrystals. For example, it was presented in Shershulin et al.

TABLE 10.1 Estimation of the sp^3 diamond carbon and noncarbon present in the differently chemically modified detonation nanodiamonds (DND) (Reineck et al., 2017).

Sample	sp^3 diamond (wt.%)	sp^2 and nondiamond sp^3 carbon (wt.%)
DND	81	19
Octadecylamine DND (DND-ODA)	74	26
Ethylenediamine DND (DND-EDA)	83	17
Hydrogenated DND (DND-H)	70	30
Hydroxylated (DND-OH)	76	24
Carboxylate DND (DND-COOH)	94	6

Source: From Reineck, P., Lau, D.W.M., Wilson, E.R., Fox, K., Field, M.R., Deeleepojananan, C., Mochalin, V.N. Gibson, B.C. (2017). Effect of Surface Chemistry on the Fluorescence of Detonation Nanodiamonds. *ACS Nano, 11*(11), 10924–10934. https://doi.org/10.1021/acsnano.7b04647.

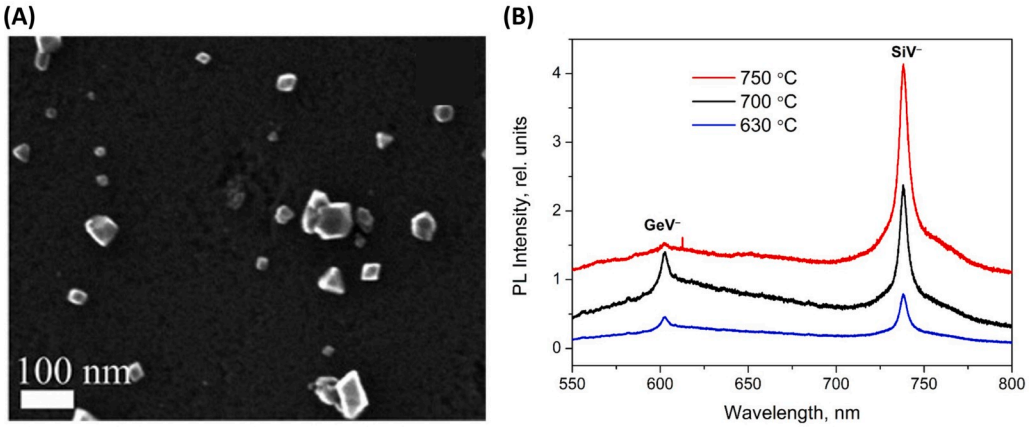

FIGURE 10.4 CVD-grown nanodiamonds. (A) The typical electron image of CVD-grown nanodiamonds (Shershulin et al., 2015). (B) The example of fluorescent spectra for CVD nanodiamonds containing two color centers simultaneously (Bogdanov et al., 2022).
Source: From Shershulin, V.A., Sedov, V.S., Ermakova, A., Jantzen, U., Rogers, L., Huhlina, A.A., Teverovskaya, E.G., Ralchenko, V.G., Jelezko, F. & Vlasov, I.I. (2015). Size-dependent luminescence of color centers in composite nanodiamonds. *Physica Status Solidi (A) Applications and Materials Science, 212*(11), 2600–2605. https://doi.org/10.1002/pssa.201532204. From Bogdanov, K.V., Baranov, M.A., Feoktistov, N.A., Kaliya, I.E., Golubev, V.G., Grudinkin, S.A. & Baranov, A.V. (2022). Duo Emission of CVD Nanodiamonds Doped by SiV and GeV Color Centers: Effects of Growth Conditions. *Materials, 15*(10), 3589. https://doi.org/10.3390/ma15103589.

(2015) that nanodiamonds with one type of color center (particularly, nitrogen-vacancy) can be overgrown with a layer containing another type of optically active defect (namely, silicon-vacancy). It was also demonstrated recently that SiV centers could be combined with germanium-vacancy (GeV) centers within the same CVD nanodiamonds (Fig. 10.4, B) (Bogdanov et al., 2022). However, the properties of CVD nanodiamonds are relatively good; they have certain limitations, mainly related to the substrates used for the growth. As mentioned before, silicon plates can be used, but in this case, nanocrystals will always be contaminated with silicon-related impurities (Shershulin et al., 2015). Other works have also reported the formation of CVD nanodiamonds on a copper substrate (Gottlieb et al., 2016) and a silicon one covered with a chromium layer (Degutis et al., 2016). Such approaches can help to avoid unwanted impurities.

The disadvantage of such a method is that nanodiamonds can hardly be removed from the substrate.Even when the removal is possible, the yield of such a technique is relatively low compared to other methods, which will be discussed later. Therefore, it limits potential applications of CVD nanodiamonds, asfluorescent nanodiamonds are often required in solution form for various applications.

10.2.4 High-pressure high-temperature nanodiamonds

The most promising bottom-up technique for nanodiamond fabrication is high-pressure high-temperature (HPHT) synthesis. This method is very similar to natural diamond formation. Here, diamond crystals are produced from graphite or other carbon-containing material. To achieve this, pressure and temperatures in the HPHT chamber must be maintained above the diamond synthesis line in Fig. 10.1. In the case of nanodiamond growth, the HPHT formation happens in a relatively short time (Stehlik et al., 2015) in comparison with bulk diamond growth (Bundy et al., 1955).

The advantage of HPHT nanodiamond synthesis is a high yield from one growth run, a shape resembling that of a large diamond crystal, and a relatively homogeneous size (Fig. 10.5B) (Crane et al., 2019). The initial carbon material for further nanodiamond formation can vary from pure graphite powder to different diamond-like molecules (e.g., adamantane) (Shenderova et al., 2019; Stehlik et al., 2015). These molecules can be mixed with other molecules or functionalized with specific atoms that need to be introduced into the diamond crystal as active impurities (Fig. 10.5, A) (Stehlik et al., 2015). Modifying the initial carbon material enables control over defect formation. For example, it was demonstrated by Davydov et al. (2014, 2016) that adding octafluoronaphthalene ($C_{10}F_8$) helps to reduce nitrogen-related defects in nanodiamonds. Nevertheless, nitrogen is the most common defect in diamonds, and it is difficult to remove it completely. Various catalytic materials can be used to initiate HPHT nanodiamond formation all around the chamber volume. The historically traditional one is catalytic metals like Ni, Fe, etc. (Bovenkerk et al., 1959; Bundy et al., 1955). Their presence stimulates the nanodiamond formation; however, they also can be introduced into the diamond lattice and become parasitic defects. Metal-free HPHT nanodiamonds synthesis can be realized using ultrasmall detonation nanodiamonds as seeds for large nanocrystal formation (Davydov et al., 2014, 2016; Stehlik et al., 2015).

There is a significant interest in synthesizing HPHT nanodiamonds under the middle temperature and high pressure (Alkahtani et al., 2018; Liang et al., 2020). This approach was motivated by the idea of using adamantane molecules as

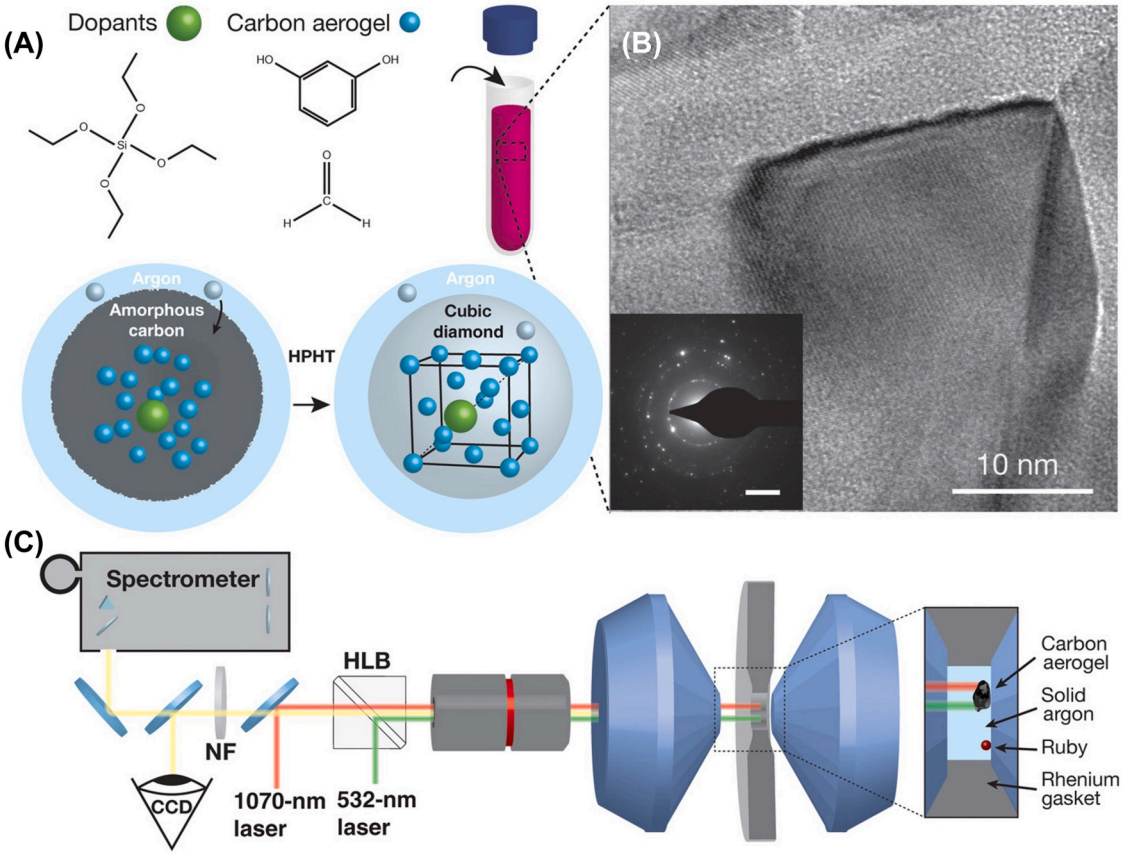

FIGURE 10.5 HPHT nanodiamonds. (A) Schematic representing the synthesis and doping of carbon aerogels (Crane et al., 2019). (B) Scanning transmission electron microscope imaging of the HPHT nanodiamond material (Crane et al., 2019). (C) Schematic showing diamond anvil cell to produce HPHT nanodiamonds with a control possibility by Raman and photoluminescence spectroscopy. All images are from Crane et al. (2019)
Source: From Crane, M. J., Petrone, A., Beck, R. A., Lim, M. B., Zhou, X., Li, X., Stroud, R. M. & Pauzauskie, P. J. (2019). High-pressure, high-temperature molecular doping of nanodiamond. *Science Advances, 5*(5), eaau6073. https://doi.org/10.1126/sciadv.aau6073. CC-BY user license.

diamond precursor to avoid parasitic impurities. The experiment of synthesis of a low amount of HPHT nanodiamond can be made inside a diamond anvil cell (Fig. 10.5, C) (Crane et al., 2019). Such a system gives a low yield but allows the control of nanodiamond formation during growth by Raman and photoluminescence spectroscopies that reflect the conversion of sp^2 carbon to sp^3 diamond structure. For some color centers, additional vacancies can be needed. For this purpose, postsynthesis irradiation and annealing can be used for the formation of required defects.

10.2.5 Milled nanodiamonds

Nowadays, the most popular technique to fabricate nanodiamonds is a single top-down approach, in which bulk diamonds are milled to the nanoscale size (Fig. 10.6) (Boudou et al., 2013). The initial material is typically HPHT-synthesized microdiamonds with a high concentration of impurities needed for further color center creation. For instance, for nanodiamonds with nitrogen-vacancy (NV) centers, nitrogen-enriched microdiamonds are first irradiated with electrons for vacancy creation and annealed for final NV formation. After that, multiple milling and purification steps are performed. This method enables the large-scale, cost-effective, and rapid production of nanodiamonds while allowing for the creation of various color centers. Obtained nanodiamonds can be easily dispersed in a suspension for further applications. Nevertheless, purification and centrifugation steps allow the separation of nanodiamonds with different sizes, the final distribution stays quite broad.

Another issue with milled nanodiamonds is their shape. With high probability, milled nanodiamonds are elongated in one dimension in contrast to more "round" HPHT nanocrystals. Thus results in a situation when color centers are located near the surface or at the nanocrystal edge. It can negatively affect the fluorescence and spin properties of optically active defects in milled nanodiamonds. At the same time, it is difficult to produce milled nanodiamonds with complete uniform size and shape.

10.3 Color centers in nanodiamonds

The nature of fluorescence coming from nanodiamonds can be related to amorphous sp^2 carbon structures on the diamond surface or structural defects within the diamond crystal, particularly color centers. These two types of fluorescence demonstrate significant differences in the case of photostability, spectral stability, lifetime, etc. Therefore, it determines the application areas of different types of fluorescent nanodiamonds.

The fluorescence corresponding to the presence of amorphous sp^2 carbon (Fig. 10.7) (Reineck et al., 2017) is similar to emission from graphite powder or carbon nanoparticles (Fig. 10.8) (Shang et al., 2012). This is common in detonation nanodiamonds, where sp^2 carbon is the primary source of fluorescence. As previously discussed, amorphic carbon can be up to 30 % of detonation nanodiamonds (Reineck et al., 2017). Such emission is characterized by a broad spectrum strongly dependent on the surface treatment and presented chemical groups (Fig. 10.7) (Reineck et al., 2017). As we can see, the fluorescent maximum of detonation nanodiamonds with different surface functionalization can vary from approximately 525 nm for ethylenediamine functionalized nanodiamonds (DND-EDA) to 650–675 nm for hydrogenated (DND-H) or carboxylated (DND-COOH) detonation nanocrystals. Let's compare the emission spectra of detonation nanodiamonds with fluorescence related to NV centers. We see the presence of additional fluorescence that is shifted in the blue area (Fig. 10.7). The intensity of sp^2-related fluorescence strongly depends on the total amount of sp^2 carbon. Therefore, for detonation nanodiamonds, the fluorescence intensity dramatically depends on surface modification (Fig. 10.7) (Reineck et al., 2017). Surface modification of detonation nanodiamonds also affects their time-resolved fluorescence decay and photobleaching (Fig. 10.7). However, it is important to note that sp^2-related fluorescence is quickly photobleached. This significantly limits the applications of nanodiamonds with this type of fluorescence, making them unsuitable for photonics.

The alternative type of fluorescence in nanodiamonds is related to structural defects, known as color centers. Currently, more than 500 optically active defects are known. However, only a few have been thoroughly studied (Zaitsev, 2001). The optical properties of nanodiamonds are determined by crystal defects and are independent of their size and shape, in contrast to other fluorescent nanoparticles such as metal nanoparticles or quantum dots (Shenderova et al., 2019). The structure and charge states of these color centers determine their fluorescent spectra. The most commom defect in fluorescent nanodiamonds is an NV center that consists of a substitutional nitrogen atom next to a vacancy. It is explained by the fact that NV centers are easy to fabricate. During the last few years, the fabrication of nanodiamonds with SiV centers, where an interstitial silicon atom is surrounded by two vacancies, has been significantly improved. They have also become attractive for different applications, including photonics and nanoscale thermometry. Nanodiamonds with GeV centers, which have a similar structure to SiV centers but with a germanium atom instead, also attract much attention due

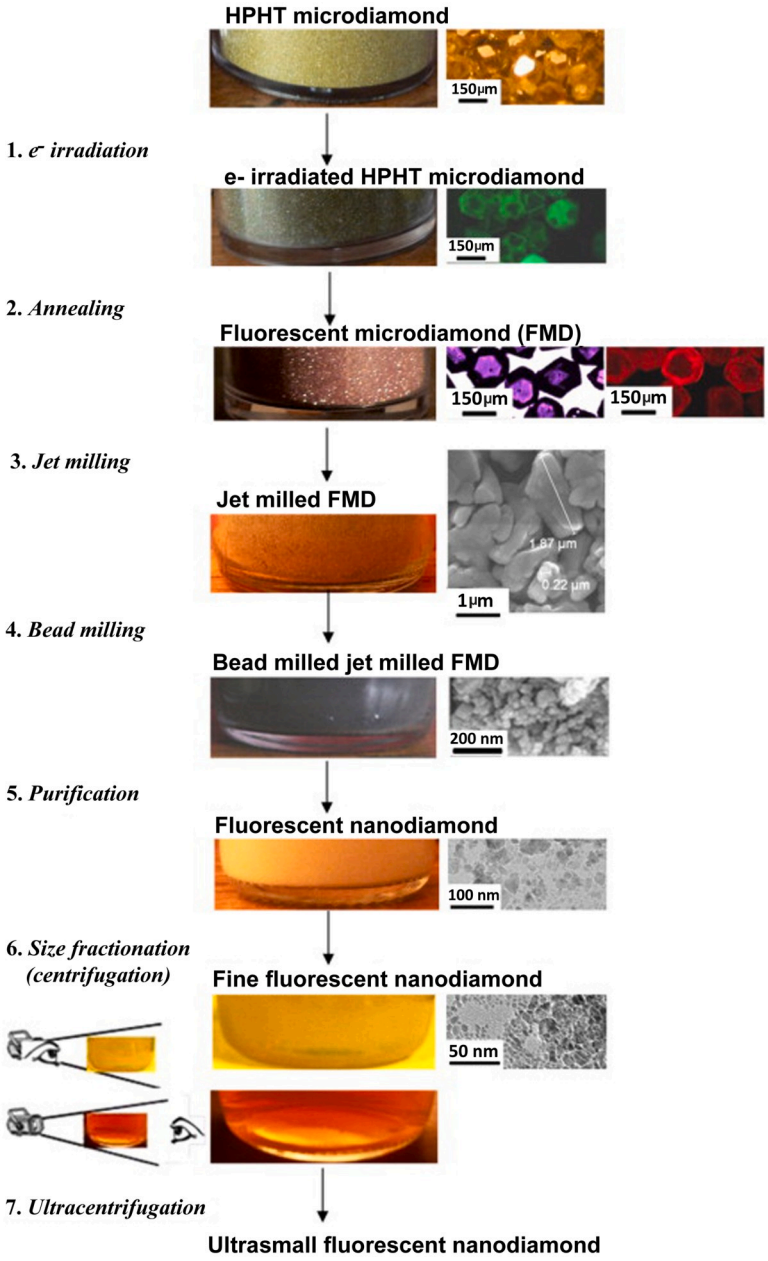

FIGURE 10.6 Fabrication of milled nanodiamonds. Schematic illustration of steps to fabricate milled fluorescent nanodiamonds from the microdiamonds. All images are from Boudou et al. (2013).
Source: From Boudou, J.P., Tisler, J., Reuter, R., Thorel, A., Curmi, P.A., Jelezko, F. & Wrachtrup, J. (2013). Fluorescent nanodiamonds derived from HPHT with a size of less than 10 nm. *Diamond and Related Materials*, *37*, 80–86. https://doi.org/10.1016/j.diamond.2013.05.006.

to their spectral properties; however, their fabrication is still tricky, and performed experiments are very limited. More detailed descriptions of different color centers related to their electron structures, fabrication techniques, and optical properties can be found in Chapter 5. Here, we focus on key aspects relevant for color centers in nanodiamonds.

10.3.1 Surface of nanodiamonds

The key difference between bulk diamonds and nanocrystals is connected to the surface-to-volume ratio. It was shown that the properties of a color center are strongly dependent on its distance from the diamond surface (Hauf et al., 2011; Shershulin et al., 2015; Stehlik et al., 2018). Additionally, the surface is the largest structural defect in a crystal, affecting

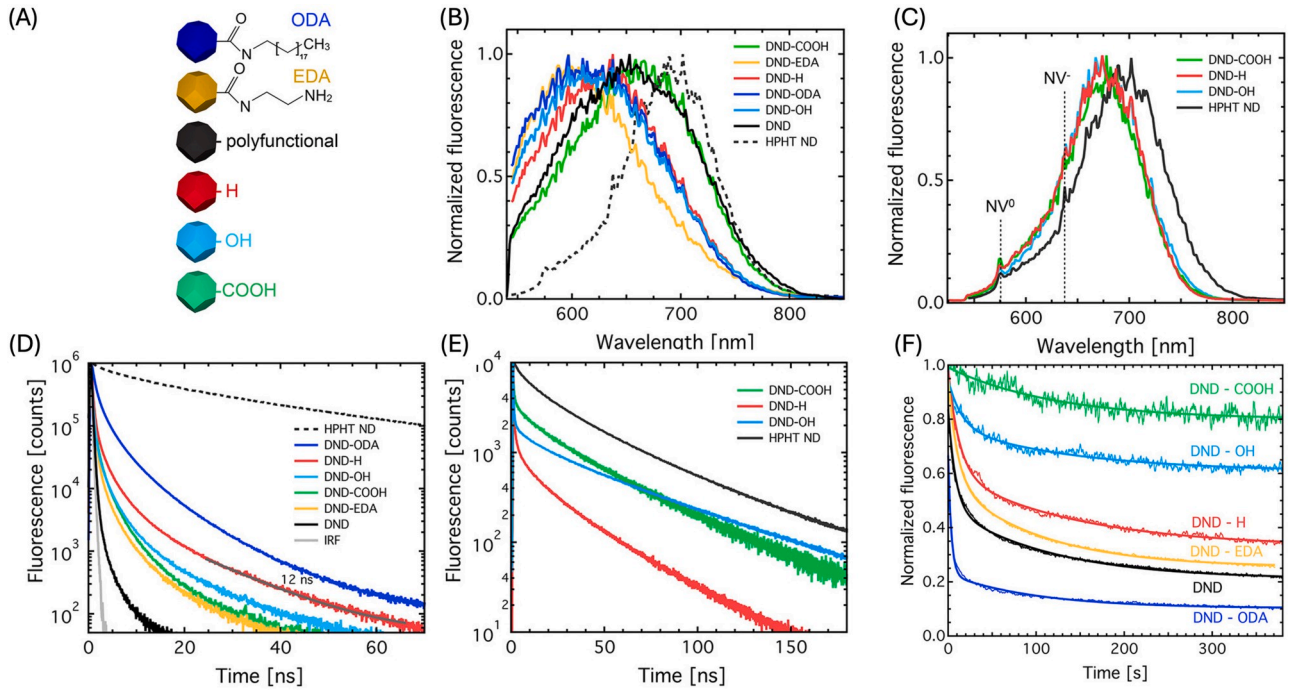

FIGURE 10.7 Color centers in nanodiamonds. (A) Detonation nanodiamonds with different surface functionalizations. Fluorescence spectra of differently functionalized detonation nanodiamonds and HPHT nanodiamonds with NV for comparison (B) in average and (C) from the individual bright spots. Time-resolved fluorescence decay traces (D) in average and (E) from the individual bright spots. (f) Normalized signal of photostability of detonation nanodiamonds with differently functionalized surfaces. All images are from Reineck et al. (2017).
Source: Adapted with permission from Reineck et al. (2017). Copyright 2017 American Chemical Society.

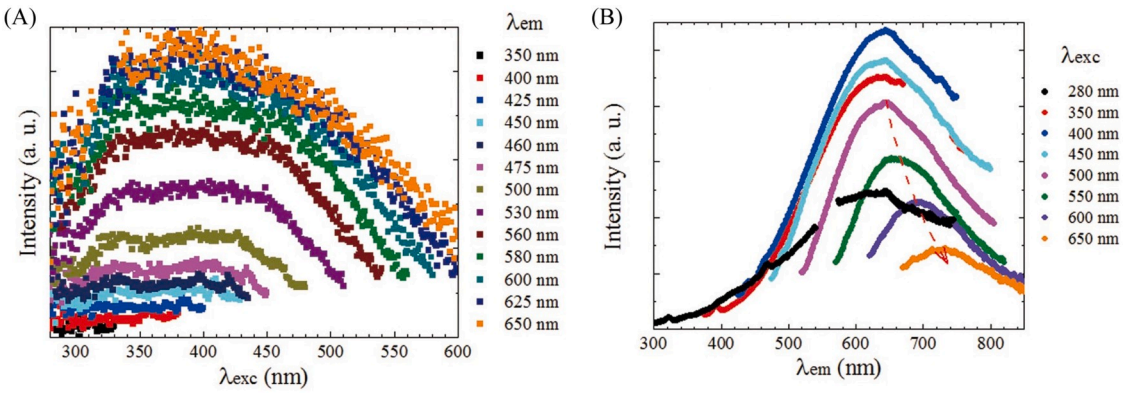

FIGURE 10.8 Spectra of graphene oxide in water. Fluorescence excitation (A) and emission (B) spectra of graphene oxide (GO) in water. All images are from Shang et al. (2012).
Source: From Shang, J., Ma, L., Li, J., Ai, W., Yu, T. & Gurzadyan, G.G. (2012). The origin of fluorescence from graphene oxide. *Scientific Reports*, *2*(1), 792. https://doi.org/10.1038/srep00792.

the linewidth and lifetime of color centers. The charge stability of color centers and, as a result, their optical properties, such as spectral characteristics and photostability, are strongly connected to the diamond surface (Hauf et al., 2011; Stehlik et al., 2018).

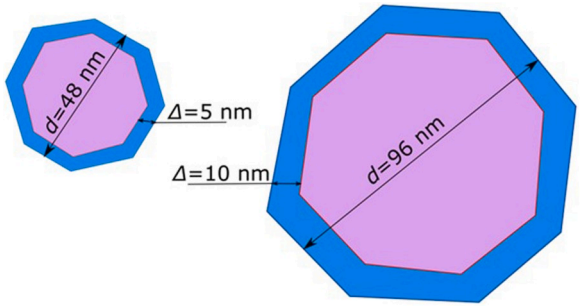

FIGURE 10.9 Probability of finding color centers in nanodiamonds. Schematic representation of nanodiamond areas close to the surface (*blue layers*) and the center (*pink cores*) with the same probability of finding an NV center according to the atom ratio in both regions.

In bulk diamonds, it is possible to probe deeper into the crystal and work with defects located at least a few tens of nm below the surface (except in ultrasensitive sensing experiments, like nanoscale NMR (Mamin et al., 2013; Staudacher et al., 2013). This is not possible for nanodiamonds, particularly when working with small and ultrasmall nanocrystals. For instance, assuming that a nanodiamond has a spherical shape with a diameter *d,* to have equal probabilities of finding a color center in the layer closer than Δ=5 nm to the surface or in the "core" part, the *d* should be 48 nm, based on volume ratio (Fig. 10.9). If Δ is 10 nm, *d* should be 96 nm. So far, for nanodiamonds smaller than 50 nm in size, color centers are predominantly located near the surface. Therefore, surface treatment and functionalization are crucial for maintaining nanodiamonds as stable emitters. A similar effect is observed for shallow color centers of a bulk diamond. Understanding proper surface modifications is essential not only for nanodiamonds but also for diamond pillars or other diamond fabricated structures.

The optical properties of color centers are determined by their electron structure (see Chapter 5). The surrounding atoms and structural defects determine the electron structure. Therefore, the exact position of the electron levels or the splitting of particular centers depend not only on the diamond crystal in its perfect structure but also on surrounding impurities and defects, including the surface. For NV centers in nanodiamonds, this leads to a splitting of spin states –1 and +1 in the ground state, typically by 10 MHz, whereas in bulk diamonds, these levels remain degenerate (Rondin et al., 2014). In the case of SiV centers, the shift of zero-phonon line position and its broadening were observed in nanodiamonds in comparison with bulk crystals (Liu et al., 2022).

Another important aspect of color centers in nanodiamonds is their charge stability. The presence of closely positioned donors or acceptors influences the charge state of a color center. However, the electron source or trapping system is not necessarily inside the crystal, it can also be at the surface. Surface termination affects the position of the Fermi level in the area close to the surface. Therefore, if a color center is located near the surface, which is a common case for nanodiamonds, as discussed earlier, its charge state and, consequently, its optical properties are sensitive to the surface's chemical state. Various types of surface modifications and their influence on color center states have been extensively investigated by different research groups.

10.3.2 Nitrogen-vacancy centers in nanodiamonds

The most investigated diamond color center is the nitrogen-vacancy (NV) defect. There are two optically active charge states of the NV center: negatively charged NV^- and neutral NV^0. They both are characterized by broad fluorescence spectra, withzero-phonon line (ZPL) positions at 637 nm for NV^- and 587 nm for NV^0 (Shenderova et al., 2019). The ratio of emitted phonon-corresponded light to ZPL emission (Debye–Waller factor) for the NV centers is 3 %–5 % independent from the charge state (Wolters et al., 2010). It was shown by Hauf et al. how different surface modifications affect the charge state of the NV center (Fig. 10.10). Particularly, the defects were switched between a negatively charged state, which is sensitive to the magnetic field, for O-terminated surface and an optically non-active state, which probably corresponded to positively charged centers, for H-termination (Hauf et al., 2011). Calculations for a better understanding of charge switching in shallow NV centers with different surface terminations were provided by Kaviani et al. (2014). Another study on charge stability of NV centers depending on the surface modification was done in 2017 by creating a radical exposure nitridation surface (Fig. 10.11) (Kageura et al., 2017). It was shown that nitrogen radical exposure improves the charge stability of shallow NV centers (Fig. 10.11). At the same time, the contrast of observed Rabi oscillations was better and sufficiently stablewith nitrogen termination than with oxygen termination (Fig. 10.11).

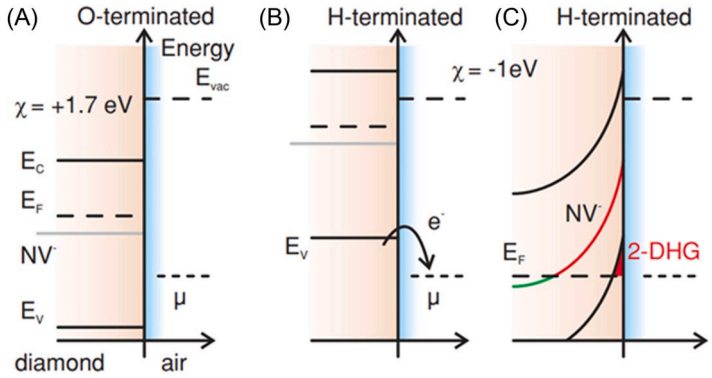

FIGURE 10.10 Representation of energy-band of diamond close to the surface area for different types of surface termination and its effect on the NV charge state. (A) Oxygen termination, (B) hydrogen termination with (C) equilibrium and identification of a two-dimensional hole gas (2-DHG) at the surface. All images are from Hauf et al. (2011).
Source: From Hauf, M. V., Grotz, B., Naydenov, B., Dankerl, M., Pezzagna, S., Meijer, J., Jelezko, F., Wrachtrup, J., Stutzmann, M., Reinhard, F. & Garrido, J. A. (2011). Chemical control of the charge state of nitrogen-vacancy centers in diamond. *Physical Review B*, *83*(8), 081304. https://doi.org/10.1103/physrevb.83.081304.

All those previously discussed types of surface terminations and their influence on the charge stability have been primarily studied for a bulk diamond. Of course, this applies even more strongly to nanodiamonds. Depending on surface modification, it was demonstrated that obtaining a pure spectrum of NV^- in nanodiamonds is almost impossible. Even for a single color center verified by antibunching measurement, fluorescence spectra would demonstrate ZPL for both optically active charge states: NV^0 and NV^-. It becomes more significant for further chemical modification of nanodiamond surfaces. When discussing samples soluble in water or other solvent, acid treatment is the first step of all nanodiamond preparations. As a standard acid solution, the mixture of three acids is used: nitric, perchloric, and sulfuric acid (triacid cleaning) in the ratio 1:1:1. It allows for obtaining a carbonylated surface that is similar to oxidized surface and supports stabilization of NV^- charge state. At the same time, the -COOH group can be used for the further chemical functionalization of nanodiamonds. For some nanodiamond functionalizations, like coating with BSA (bovine serum albumin) or HSA (human serum albumin) proteins, fluorescent properties of the NV remain stable (Wu et al., 2015). However, some surface treatment can also induce blinking of the NV centers in nanodiamonds, which is related to charge state changes (Bradac et al., 2010). Such blinking phenomena can be beneficial for certain high-resolution imaging techniques. However, for photonics, stable and predictable emitters are preferred.

10.3.3 Silicon-vacancy centers in nanodiamonds

Different types of surface modifications affect not only the NV centers but all other color centers. Nevertheless, this influence is not always fully investigated. The silicon-vacancy (SiV) center is a highly promising system for imaging and sensing in living systems due to all-optical thermometry with its negatively charged state SiV^- (Nguyen et al., 2018). It was demonstrated that fluorescent SiV centers can be found in ultrasmall nanodiamonds down to 1.6 nm (Vlasov et al., 2014). However, it is challenging to obtain nanodiamonds with a high yield of optically stable SiV centers (Jantzen et al., 2016; Shimazaki et al., 2021). Fluorescence blinking is typical for the SiV centers in nanodiamonds (Fig. 10.12). The SiV center has an optically active negatively charged state (SiV^-) with the position of ZPL at 738 nm at room temperature, with the Debey–Waller factor at 70 % (Aharonovich et al., 2011). For bulk diamonds, the fluorescence from the neutral SiV^0 center has been reported with a ZPL position at 946 nm and a Debye–Waller factor of almost 90 % (Rose et al., 2018). However, the SiV^0 centers have not been observed in nanodiamonds until now. Therefore, any charge instability of the SiV due to impurities or structural defects and surface modifications leads to fluorescence blinking or a dramatic shift of emission spectra. The production of nanodiamonds with the SiV centers can be easily done by CVD growth when silicon wafers are used as a substrate (De Feudis et al., 2020; Shershulin et al., 2015). Such a method allows the overgrowth of nanodiamonds containing other color centers; for instance, nanodiamonds with NV centers can be overgrown with an additional SiV layer (Shershulin et al., 2015). However, for many applications, nanodiamonds should be dispersed in a solution. Therefore, HPHT production of nanodiamonds with SiV centers is more preferable due to the higher possible yield. Producing nanodiamonds via HPHT without NV centers, containing only SiV centers, is somewhat challenging because nitrogen is a widespread element and can easily be incorporated into the diamond structure. However,

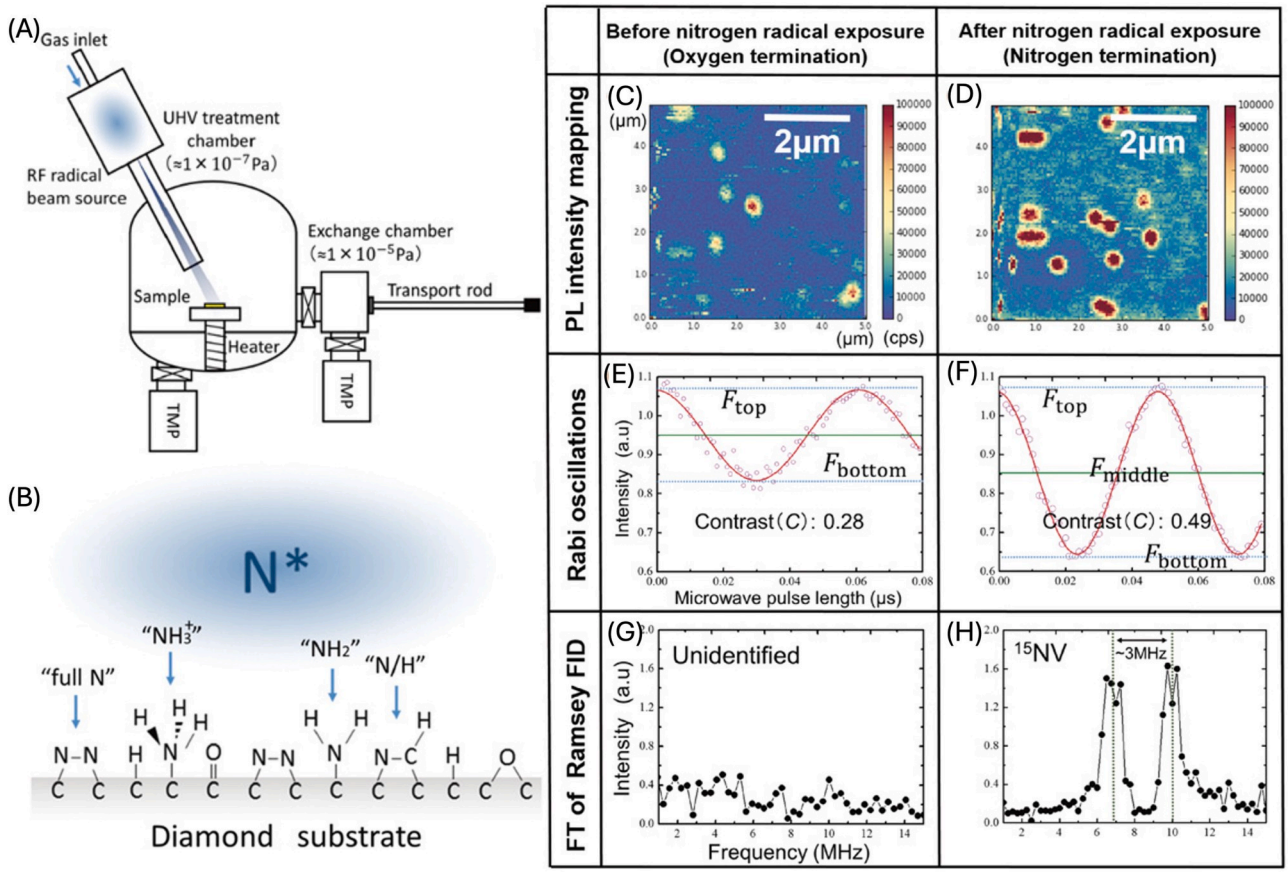

FIGURE 10.11 **Effect of radicals on NV centers in nanodiamonds.** (A) Schematic diagram of a radical exposure system and (B) types of C-N bonds (such as N, N/H, NH_2, and NH_3^+) at the surface formed by nitrogen radical exposure. Photoluminescence imaging of the NV containing diamond sample (C) with initial oxygen termination and (D) after nitrogen radical exposure. Rabi oscillations of the NV (C) before and (D) after nitrogen radical exposure. Fourier transformations of the Ramsey FID (E) before and (F) after nitrogen radical exposure. All images are from Kageura et al., 2017. Source: From Kageura, Taisuke, Kato, Kanami, Yamano, Hayate, Suaebah, Evi, Kajiya, Miki, Kawai, Sora, Inaba, Masafumi, Tanii, Takashi, Haruyama, Moriyoshi, Yamada, Keisuke, Onoda, Shinobu, Kada, Wataru, Hanaizumi, Osamu, Teraji, Tokuyuki, Isoya, Junichi, Kono, Shozo & Kawarada, Hiroshi. (2017). Effect of a radical exposure nitridation surface on the charge stability of shallow nitrogen-vacancy centers in diamond. *Applied Physics Express, 10*(5), 055503. https://doi.org/10.7567/apex.10.055503 CC-BY user license.

certain HPHT synthesis techniques allow for the production of nanodiamonds containing only the SiV centers (Davydov et al., 2014, 2016).

To investigate the surface effect on SiV centers in nanodiamonds in more detail, the team of S. Stehlik and his colleagues tested hydrogenated and oxidized terminations of ultra-small nanodiamonds (Stehlik et al., 2018). It was demonstrated that the intensity of ZPL of the SiV is higher for oxidized nanodiamonds (Fig. 10.13A). Moreover, for smaller nanodiamonds with a size of 10 nm, there was no evidence of ZFL of the SiV for hydrogenated nanodiamonds compared to oxidized (Fig. 10.13A). This phenomenon can be explained by the changes in the Fermi level for different surface terminations (Fig. 10.13B and C).

Another issue related to SiV centers in nanodiamonds is connected not only to the charge stability of the color center but also to the general optical properties of the SiV^- center, such as the position and width of the ZPL. In comparison to a bulk sample, nanodiamonds demonstrate a broader distribution in the position of the ZPL and its width (Lindner et al., 2018; Neu et al., 2011). It can be explained by the relationship between crystal strain and defects, including such a large defect as the crystal surface. Such an effect should be considered, especially in applications like all-optical thermometry with SiV centers. It was shown in the work (Liu et al., 2022) that the initial positions and width of the ZPL vary for different nanodiamonds. This affects the shift of their ZPL as a function of temperature (Fig. 10.14A). Therefore, the temperature behavior for nanodiamonds is more complex than for bulk crystals (Liu et al., 2022; Nguyen et al., 2018). As shown in

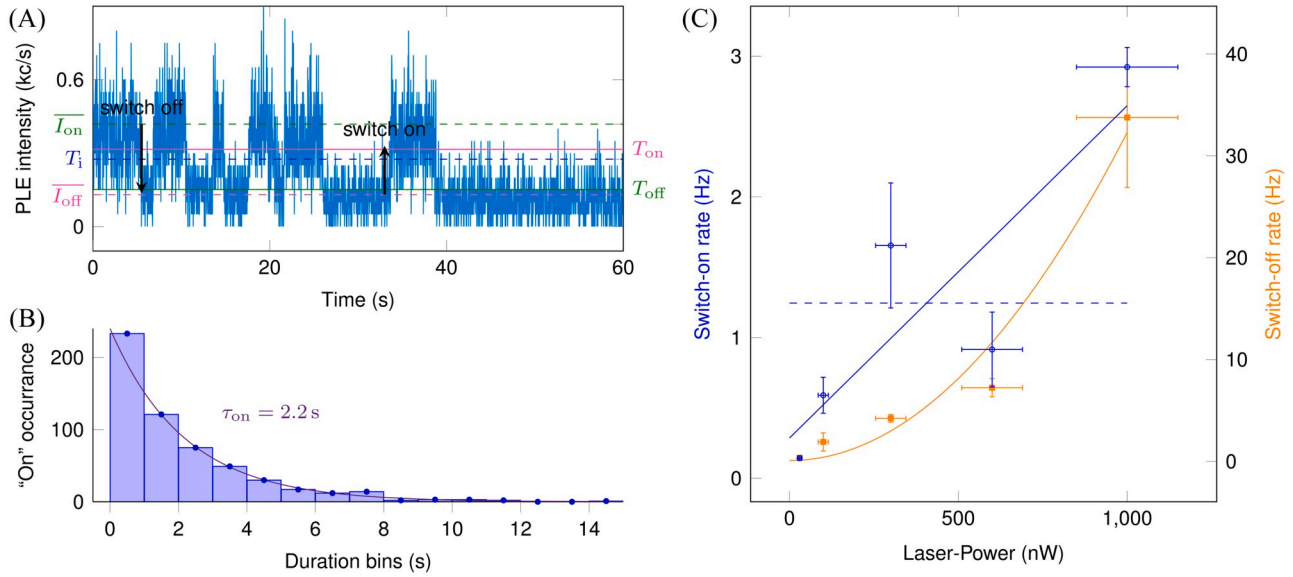

FIGURE 10.12 Blinking of SiV in nanodiamonds. Illustration of blinking behavior of the SiV in nanodiamonds. (A) Photoluminescence signal of SiV in time under resonant excitation. (B) Histograms demonstrate duration for optically "on" and "off" intervals. (C) The increasing of "on" and "off" rates (Ron and Roff) with excitation laser intensity. All images are from Jantzen et al. (2016).
Source: From Jantzen, U., Kurz, A.B., Rudnicki, D.S., Schäfermeier, C., Jahnke, K.D., Andersen, U.L., Davydov, V.A., Agafonov, V.N., Kubanek, A., Rogers, L.J. & Jelezko, F. (2016). Nanodiamonds carrying silicon-vacancy quantum emitters with almost lifetime-limited linewidths. *New Journal of Physics, 18*(7), 073036. https://doi.org/10.1088/1367-2630/18/7/073036 CC-BY user license.

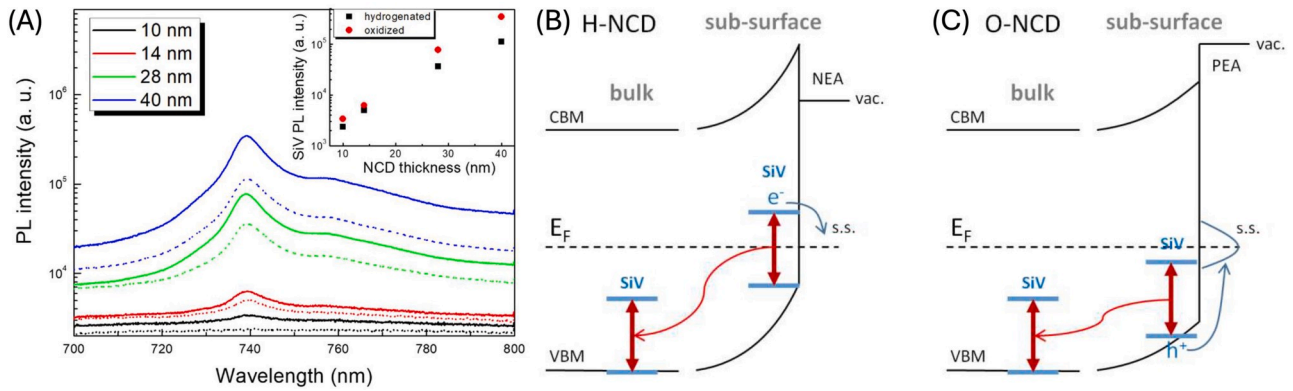

FIGURE 10.13 Surface effects on SiV in nanodiamonds. (A) Photoluminescence spectra and intensity of shallow SiV centers depending on the thickness of nanodiamond film and surface termination: hydrogenated (*dotted lines*) oxidized (*full lines*). Schematic illustration of the band gap changes for different surface modifications of nanodiamonds with the SiV: (B) hydrogenated and (C) oxidized. All images are from Stehlik et al. (2018).
Source: From Stehlik, Stepan, Ondic, Lukas, Varga, Marian, Fait, Jan, Artemenko, Anna, Glatzel, Thilo, Kromka, Alexander & Rezek, Bohuslav. (2018). Silicon-Vacancy Centers in Ultra-Thin Nanocrystalline Diamond Films. *Micromachines, 9*(6), 281. https://doi.org/10.3390/mi9060281 CC-BY user license.

Fig. 10.14, some SiV centers in nanodiamonds demonstrate more linear shifts with temperature. On the other hand, there is another group of nanodiamonds where the temperature-dependent shift of ZPL position jumps in not precise linear behavior. Therefore, it becomes an important point for nanodiamonds with SiV centers coupled to photonic structures. Additionally, the ZPL positionfor SiV centers in nanodiamonds is highly pressure-dependent, as demonstrated in the work (Vindolet et al., 2022) (Fig. 10.14B).

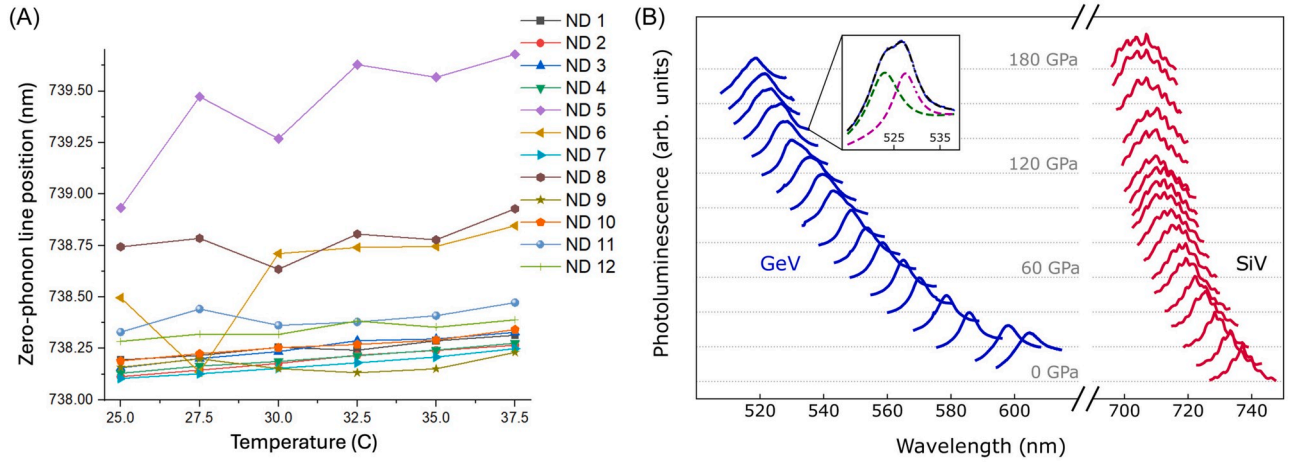

FIGURE 10.14 Temperature and pressure sensing. (A) Temperature shift of ZPL of the SiV centers in nanodiamonds. (b) Pressure dependence of the photoluminescence spectra of the GeV centers (shown in blue, left) and the SiV centers (shown in red, right) and in CVD nanodiamonds. Image (B) is from Vindolet et al. (2022).

Source: From Vindolet, B., Adam, M.P., Toraille, L., Chipaux, M., Hilberer, A., Dupuy, G., Razinkovas, L., Alkauskas, A., Thiering, G., Gali, A., De Feudis, M., Ngandeu Ngambou, M.W., Achard, J., Tallaire, A., Schmidt, M., Becher, C. & Roch, J.F. (2022). Optical properties of SiV and GeV color centers in nanodiamonds under hydrostatic pressures up to 180 GPa. *Physical Review B, 106*(21), 214109. https://doi.org/10.1103/PhysRevB.106.214109.

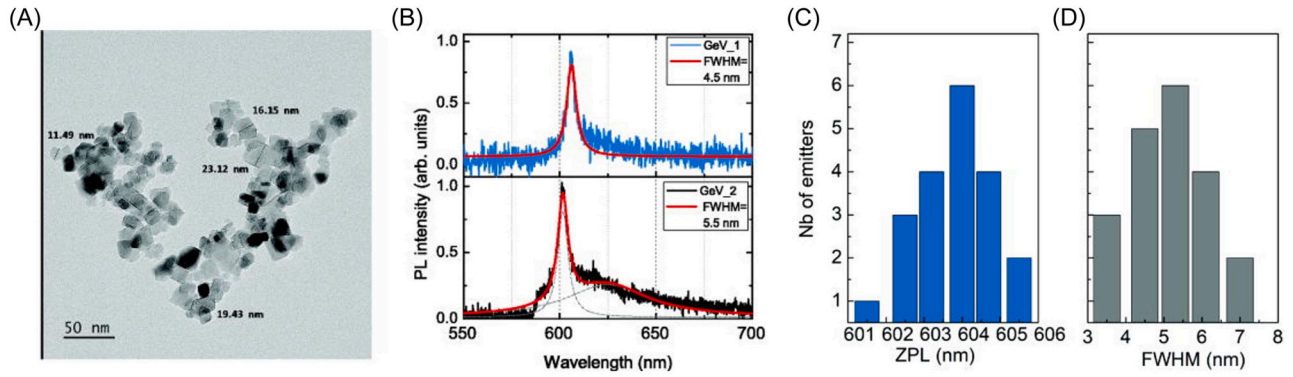

FIGURE 10.15 GeV centers in nanodiamonds. (A) Transmission electron imaging of HPHT nanodiamonds with the GeV centers, the average size is 20 nm. (B) Photoluminescence spectra of two different nanodiamonds containing the GeV centers. Histogram distributions of (C) ZPL and (D) full width at half maximum(FWHM) for 20 emitters. All images are from Nahra et al. (2021.)

Source: From Nahra, M., Alshamaa, D., Deturche, R., Davydov, V., Kulikova, L., Agafonov, V. & Couteau, C. (2021). Single germanium vacancy centers in nanodiamonds with bulk-like spectral stability. *AVS Quantum Science, 3*(1), 012001. https://doi.org/10.1116/5.0035937.

10.3.4 Germanium-vacancy centers in nanodiamonds

The bigger the impurity element is, the harder it is to incorporate into the diamond crystal. This is true for a bulk diamond and is even more critical for nanodiamonds. Synthesis of nanodiamonds with the geermanium-vacancy (GeV) centers is still challenging; however, there are a few ways to do it nowadays. The first production of GeV nanodiamonds was based on the CVD method (De Feudis et al., 2020; Vindolet et al., 2022). As previously mentioned, the amount of nanodiamonds that can be produced using the CVD technique may be insufficient, making the HPHT strategy more preferable for nanodiamond fabrication. Several methods of HPHT synthesis of nanodiamonds with GeV centers have been tried so far. The first one was the growth from adamantane and germanium iodide (Liang et al., 2020). Another and more successful way was to introduce tetraphenyl germanium during the growth process (Nahra et al., 2021). These nanodiamonds are characterized by homogeneous size distribution ranging from 10 to 50 nm (Fig. 10.15A) (Nahra et al., 2021). Surface treatment of such nanodiamonds was performed to remove residual germanium and germanium oxide. Nanodiamonds

were heated up to 160 °C for two hours in hydrofluoric acid and then dissolved in a mixture of ultrapure water and isopropanol. A sharp ZPL emission of the GeV centers was observed, sometimes accompanied by background fluorescence (Fig. 10.15B) (Nahra et al., 2021). This background emission may result from amorphous carbon on the nanodiamond surface. The distribution of the position and the width of ZPL of the GeV centers in these HPHT nanodiamonds are also shown in Fig. 10.15C.

The investigation of the surface treatment influence on GeV centers in nanodiamonds has not yet been thoroughly investigated. However, based on previous research of such color centers as NV and SiV, we can expect that surface modification will also play a significant role.

There are other color centers that are potentially attractive for photonics, namely tin-vacancy (SnV) (Iwasaki et al., 2017; Tchernij et al., 2017) and lead-vacancy (PbV) defects (Ditalia Tchernij et al., 2018; Trusheim et al., 2019). The synthesis of nanodiamonds containing the SnV and the PbV centers has naturally attracted significant attention. The first steps in this direction were done to produce SnV nanodiamonds using CVD (Westerhausen et al., 2020) and detonation (Makino et al., 2022) techniques. So far, nanodiamonds with PbV centers have only been obtained by the detonation method (Makino et al., 2022). The characteristic fluorescent spectra of these color centers in nanodiamonds have been demonstrated. However, a deeper investigation of their stability, line broadening, and surface influence still needs to be done.

Nanodiamonds with color centers offer vast potential for sensing applications that stay out of the focus of this chapter. However, the information about sensing with nanodiamonds can be found in the following papers: magnetic field sensing (Alkahtani et al., 2018; Shenderova et al., 2019), pH detection (Fujisaku et al., 2019), thermometry with the NV (Plakhotnik et al., 2014), SiV (Liu et al., 2022), and GeV (Chen et al., 2023), among others. Photonic applications of fluorescent nanodiamonds are strongly influenced by the sensitivity of color centers to surface charges, including pH dependence, as this affects their optical properties (Fujisaku et al., 2019). Additionally, it is important to consider that the ZPL position is temperature- and pressure-dependent (Liu et al., 2022; Vindolet et al., 2022). Therefore, the design of photonic systems with fluorescent nanodiamonds should consider their surface modifications and thermal stability to mitigate potential negative effects.

10.4 Photonics integration

Fluorescent nanodiamonds are promising emitters for integration with photonic cavities. In the last few years, a couple of wonderful reviews have been published regarding this topic, for example (Radulaski et al., 2019; Sahoo et al., 2023). Here, we will briefly discuss color centers as emission sources for nanophotonic applications, where one of the most important parameters is the Debye–Waller factor. As discussed previously, the Debye–Waller factor for diamond color centers is as follows: NV - 3–5 % (Wolters et al., 2010), SiV^- - 70 % (Aharonovich et al., 2011), GeV - 60 % (Siyushev et al., 2017), and SnV- 40 % (Thiering & Gali, 2018). The integration of fluorescent nanodiamonds has been made intovarious systems, ranging from optical fibers to photonics cavities on GaP or silicon-related material.

10.4.1 Fluorescent nanodiamonds and fiber-based resonators

One of the first integrations of fluorescent nanodiamonds with photonic structures at room temperature was achieved in 2008 (Schietinger et al., 2008). Nanodiamonds, with a size of 25 nm, were coupled as single phonon emitters to high-Q whispering-gallery modes. The authors used polystyrene microspheres as microresonators (Fig. 10.16A). The single-phonon sources were confirmed by second-order correlation function, $g^{(2)}(t)$ (Fig. 10.16B). As previously discussed for a single NV center proven by antibunching measurements, both charge states (neutral and negative) were observed in the spectra (Fig. 10.16B). In this work, the authors did not mention any surface modification of nanodiamonds. There were two configurations: one nanodiamond coupled to polystyrene microspheres and two nanodiamonds coupled to the resonator. The spectra of a system with two emitter (two nanodiamonds) are shown in Fig. 10.16C. These nanodiamonds can be addressed individually.

The coupling of fluorescent nanodiamonds with fiber-based systems was demonstrated in the work of Schröder et al. (2012). Initially, individual nanodiamonds containing NV centers were placed on a trapped fiber with a diameter of 273 nm (Fig. 10.17A). This was achieved by moving the fiber through a droplet of nanodiamond solution. The deposition of diamond nanocrystals was monitored using the laser scattering signal (Fig. 10.17B). Such a system allows fluorescence collection either through an objective or at the fiber ends (Fig. 10.17C). The light observed through the fiber demonstrated redshifted spectra compared to fluorescence collected by the objective, due to the chromatic dependence of the fiber filter stage transmission. An example of saturation measurement of the NV center is presented in Fig. 10.17D. The calculated

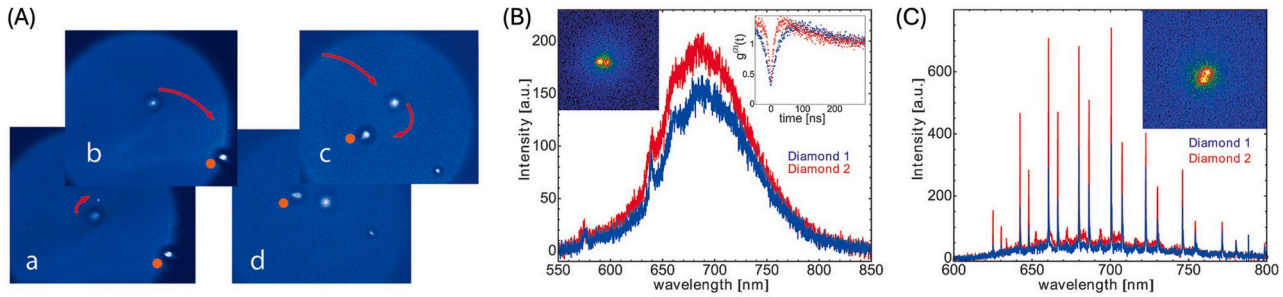

FIGURE 10.16 **Nanodiamonds coupled to microspheres.** (A) Coupling of two nanodiamonds to one polystyrene microsphere as microresonators: white (A)–(D) demonstrate the process of positioning nanodiamonds at the sphere. (B) Fluorescence spectra of two nanodiamonds placed at the coverslip with their antibunching measurements in the right top corner ($g^{(2)}$(t) functions). (C) Fluorescence spectra of the same nanodiamonds already attached to the microresonator and individually excited by the focused laser. The picture insets demonstrate that the nanodiamonds excited simultaneously with the laser. All images are from Schietinger et al. (2008).

Source: Reprinted (adapted) with permission from Schietinger, S., Schröder, T. & Benson, O. (2008). One-by-one coupling of single defect centers in nanodiamonds to high-Q modes of an optical microresonator. *Nano Letters*, *8*(11), 3911–3915. https://doi.org/10.1021/nl8023627 Copyright 2008 American Chemical Society.

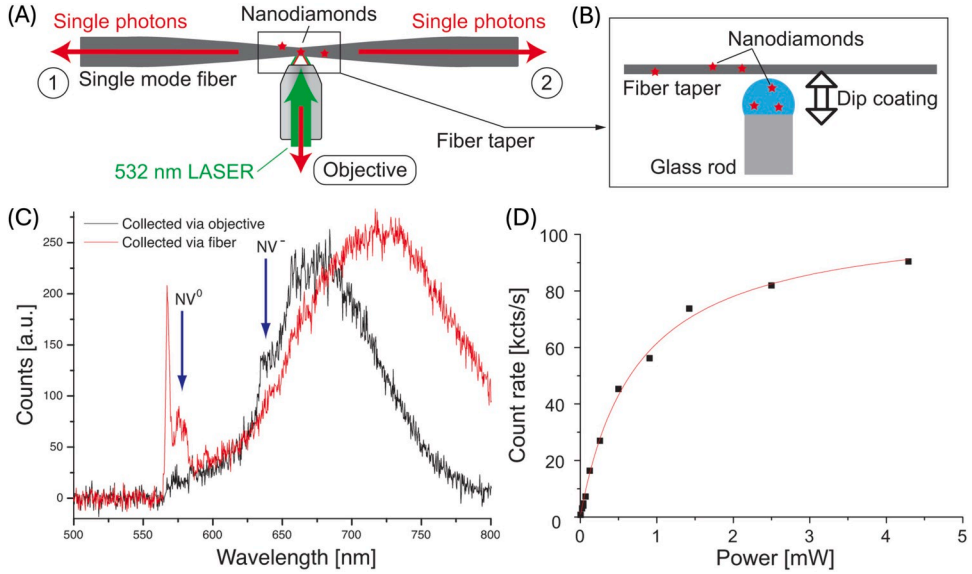

FIGURE 10.17 **Nanodiamonds coupled to tapered fibers.** (A) Schematic illustration of nanodiamond on a tapered fiber (B) by dipping it into the solution with fluorescent nanodiamonds. (C) Fluorescent spectra of several NV centers emitting light, the clear presence of both ZPL for the NV^0 and NV^- centers. (D) Saturation measurements of the coupled NV nanodiamonds. All images are from Schröder et al. (2012).

Source: Reprinted with permission from Schröder, T., Fujiwara, M., Noda, T., Zhao, H. Q., Benson, O., & Takeuchi, S. (2012). A nanodiamond-tapered fiber system with high single-mode coupling efficiency. *Optics Express*, *20*(10), 10490–10497. https://doi.org/10.1364/OE.20.010490 © The Optical Society.

photon collection efficiency allowed an estimation of the total number of single photons coupled to the single-mode fiber as 689 ± 12 x10^3 at saturation intensities (Schröder et al., 2012).

The coupling of a single NV center in nanodiamond to a fiber-based Fabry–Perot cavity operating at room temperature was demonstrated in 2013 by the group of C. Becher (Albrecht et al., 2013). In this work, the cavity was based on a plane dielectric mirror with spin-coated nanodiamonds and an optical fiber facet with a dielectric coating (Fig. 10.18A). Such geometry allowed for simple tuning of the cavity and continuous variation of the emitter-cavity coupling. The main challenge of NV coupling is related to its broad emission bandwidth. The variable cavity distance enabled the selection of

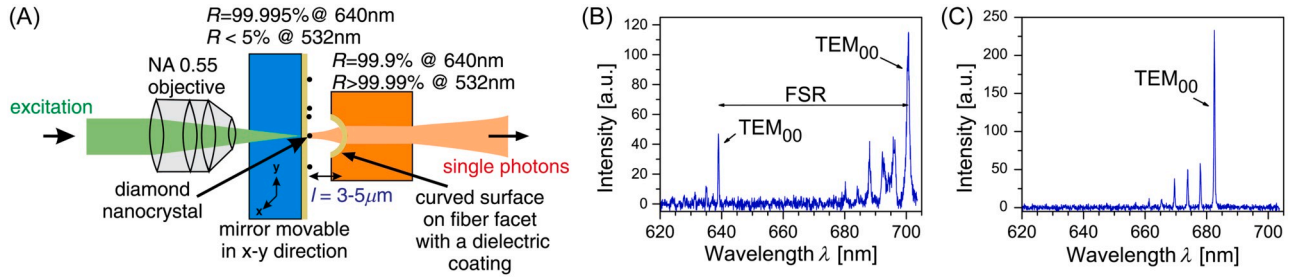

FIGURE 10.18 Nanodiamonds coupled to fiber-based Fabry-Perot cavity. (A) Schematic illustration of Fabry-Perot cavity consisting of a concave mirror on a fiber facet and a plane mirror with spin-coated nanodiamonds. Cavity emission spectra at effective cavity lengths (B) l = 3.5 μm and (C) l = 3.1 μm, where FSR is the free spectral range, TEM_{00} – the fundamental transversal modes. All images are from Albrecht et al. (2013).
Source: From Albrecht, R., Bommer, A., Deutsch, C., Reichel, J. & Becher, C. (2013). Coupling of a single nitrogen-vacancy center in diamond to a fiber-based microcavity. *Physical Review Letters, 110*(24), 243602. https://doi.org/10.1103/PhysRevLett.110.243602.

the emission spectrum, aligning with the ZPL and all phonon sideband contributions (Fig. 10.18B and C). There, the cavity finesse was limited by scattering losses from nanodiamonds. The authors proposed that smaller nanodiamonds could increase the finesse by a factor of 10 (Albrecht et al., 2013).

An alternative to the NV center in nanodiamonds for effective cavity coupling is the SiV center. The SiV spectrum consists mainly of ZPL-related emissions. As mentioned above, the Debye–Waller factor for SiV^- is approximately 70 % (Aharonovich et al., 2011). At room temperature, all four transitions merge into a single broad ZPL line with a central position at 738 nm. In 2017, nanodiamonds with SiV centers were integrated with a fiber-based microcavity (Fig. 10.19) (Benedikter et al., 2017). Different nanodiamonds were tested in that work; their spectra are shown in Fig. 10.19. For resonant coupling with SiV, the cavity length was tuned to shift a cavity resonance across the emission spectrum, similar to the NV experiments (Albrecht et al., 2013). As a result, the significant Purcell enhancement of the single-photon source based on the SiV center was demonstrated. The integration of SiV-containing nanodiamonds with fiber-based microcavity was further developed at cryogenic temperatures for potential applications in long-lived quantum memories (Bayer et al., 2022; Salz et al., 2020). GeV centers in nanodiamonds have also attracted considerable attention due to their spectral properties. Recently, the first work demonstrating the integration of a GeV center in nanodiamond with a Fabry-Perot microcavity under ambient conditions was published (Feuchtmayr et al., 2023). Further investigation of such photonic systems for practical applications, as well asunderstanding the properties of nanodiamonds containing other group VI-defects, remains necessary.

10.4.2 Fluorescent nanodiamonds and photonic crystal cavities

Various photonic crystal cavities represent another type of photonic system integrated with fluorescent nanodiamonds. In 2010, J. Wolters and his colleagues published a paper about the enhancement of the ZPL of a single NV center in nanodiamonds via coupling to a gallium phosphide (GaP) photonic crystal cavity (Fig. 10.20). The fabricated cavities had resonances around 642 nm, with a typical deviation of ± 2 nm. Preselected nanodiamonds containing single NV centers were transferred to the GaP surface by being picked up with an atomic force microscope (Fig. 10.20). It was done in two steps: first, rough localization of the nanodiamonds on the GaP cavity, followed by final, precise placement at the centers of the cavity. As a result, the deterministic coupling of the ZPL of a single NV center to the photonic crystal cavity was demonstrated (Fig. 10.20). That experiment with controled placement of fluorescent nanodiamonds at the center of the photonic crystal cavity became a foundational step toward the further developmentof quantum information processing.

10.5 Summary

Fluorescent nanodiamonds are attention-grabbing materials with potentially wide applications, from imaging and sensing to quantum computing and quantum communication. Their fluorescence originates from two primary mechanisms: amorphous sp^2 carbon on the surface or optically active crystal defects known as color centers. The unique optical properties of such color centers, particularly their emission characteristics, make nanodiamonds attractive for diverse technological applications. One of the key distinctions between bulk diamonds and nanodiamonds is the significant influence of surface properties on the fluorescence behavior of color centers. In bulk diamonds, color centers can be

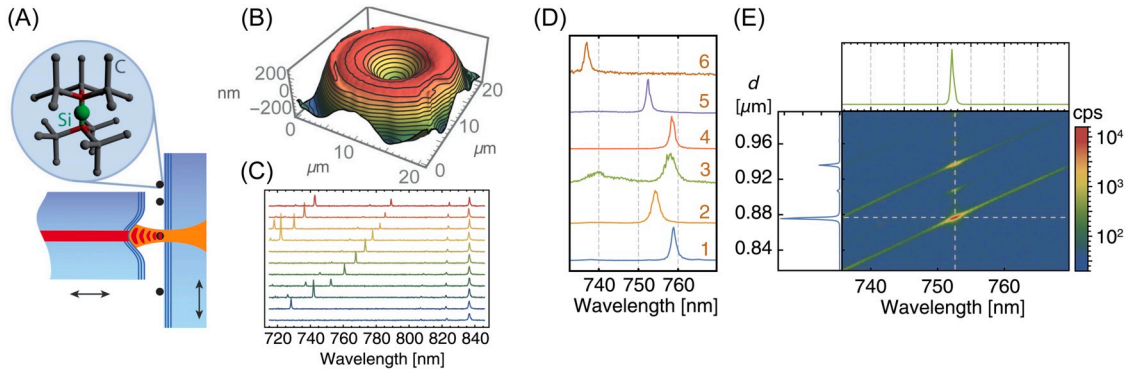

FIGURE 10.19 SiV in nanodiamond coupled to a cavity. (A) Schematic figure of a cavity and a SiV center in a diamond lattice. (B) Presenting of interferometric measurement of fiber profile. (C) Transmission spectra of the cavity for different lengths from $d = 5\lambda/2$ (the lowest curve) with steps of one free spectral range. (D) Free-space fluorescence spectra of single SiV centers studied for cavity coupling. (E) Cavity fluorescence spectra of selected nanodiamonds for different geometric cavity lengths. All images are from Benedikter et al. (2017).

Source: From Benedikter, J., Kaupp, H., Hümmer, T., Liang, Y., Bommer, A., Becher, C., Krueger, A., Smith, J.M., Hänsch, T. W., & Hunger, D. (2017). Cavity-enhanced single-photon source based on the silicon-vacancy center in diamond. *Physical Review Applied*, *7*(2), 024031. https://doi.org/10.1103/PhysRevApplied.7.024031.

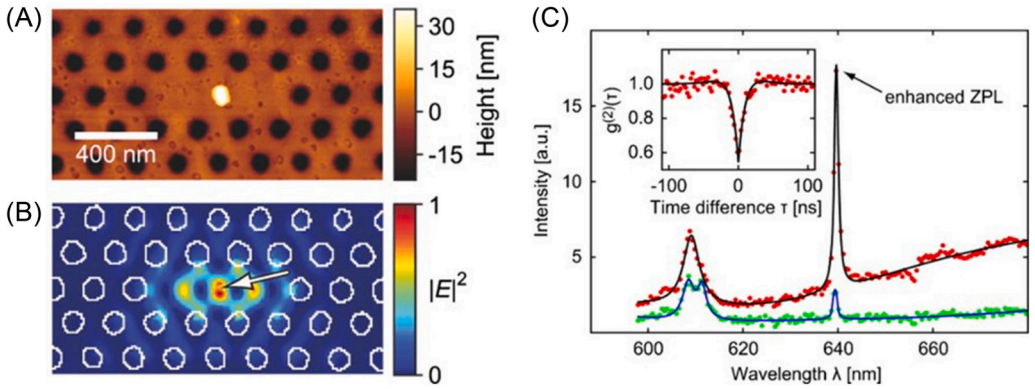

FIGURE 10.20 Nanodiamonds coupled to photonic crystal cavity. (A) AFM image of the GaP photonic crystal cavity with a nanodiamond located close to the center. The nanodiamond height is 35 nm. The lattice constant is 200 nm. (B) The profile of the simulated electric field of the fundamental mode of this cavity with geometry from (A). (C) Normalized spectra of the cavity fluorescence without (green dots) and with (red dots) nanodiamonds. Inset: Antibunching measurement of the cavity with nanodiamond. All images are from Wolters et al. (2010).

Source: From Wolters, J., Schell, A. W., Kewes, G., Nüsse, N., Schoengen, M., Döscher, H., Hannappel, T., Löchel, B. & Barth, M. (2010). Enhancement of the zero phonon line emission from a single nitrogen vacancy center in a nanodiamond via coupling to a photonic crystal cavity. *Applied Physics Letters, 97*(14), 141108. https://doi.org/10.1063/1.3499300.

positioned deep within the crystal, minimizing surface effects. However, in nanodiamonds, the surface plays a crucial role in determining charge stability and emission spectra. Surface modifications, such as chemical functionalization, are essential tools for tuning and optimizing these properties. While surface treatment allows for improved control over fluorescence and stability, it also presents challenges. Color centers in nanodiamonds are highly sensitive to surface conditions, which can lead to their charge instability, causing fluorescence blinking. Similar issues are observed for shallow color centers in bulk diamonds. The surface treatment adjustment should be done in response to a particular type of diamond color centers. Therefore, understanding and controlling the nanodiamond surface is not only important for their various applications but also relevant for engineered diamond-based photonic structures. Ultimately, the ability to manipulate the optical properties of fluorescent nanodiamonds through surface treatment has profound implications for their integration into photonic structures.

References

Aharonovich, I., Castelletto, S., Simpson, D. A., Su, C.-H., Greentree, A. D., & Prawer, S. (2011). Diamond-based single-photon emitters. *Reports on Progress in Physics, 74*(7), 076501. https://doi.org/10.1088/0034-4885/74/7/076501.

Albrecht, R., Bommer, A., Deutsch, C., Reichel, J., & Becher, C. (2013). Coupling of a single nitrogen-vacancy center in diamond to a fiber-based microcavity. *Physical Review Letters, 110*(24), 243602. https://doi.org/10.1103/PhysRevLett.110.243602.

Alivisatos, A. P. (1996). Semiconductor clusters, nanocrystals, and quantum dots. *Science (New York, N.Y.), 271*(5251), 933–937. https://doi.org/10.1126/science.271.5251.933.

Alkahtani, M. H., Alghannam, F., Jiang, L., Almethen, A., Rampersaud, A. A., Brick, R., Gomes, C. L., Scully, M. O., & Hemmer, P. R. (2018). Fluorescent nanodiamonds: Past, present, and future. *Nanophotonics, 7*(8), 1423–1453. https://doi.org/10.1515/nanoph-2018-0025.

Baitinger, E. M., Belenkov, E. A., Brzhezinskaya, M. M., & Greshnyakov, V. A. (2012). Specific features of the structure of detonation nanodiamonds from results of electron microscopy investigations. *Physics of the Solid State, 54*(8), 1715–1722. https://doi.org/10.1134/s1063783412080057.

Bayer, G., Berghaus, R., Sachero, S., Filipovski, A. B., Antoniuk, L., Lettner, N., Waltrich, R., Klotz, M., Maier, P., Agafonov, V., & Kubanek, A. (2022). A Quantum Repeater Platform based on Single SiV^- Centers in Diamond with Cavity-Assisted, All-Optical Spin Access and Fast Coherent Driving. *arXiv*. https://doi.org/10.48550/arXiv.2210.16157.

Benedikter, J., Kaupp, H., Hümmer, T., Liang, Y., Bommer, A., Becher, C., Krueger, A., Smith, J. M., Hänsch, T. W., & Hunger, D. (2017). Cavity-enhanced single-photon source based on the silicon-vacancy center in diamond. *Physical Review Applied, 7*(2), 024031. https://doi.org/10.1103/PhysRevApplied.7.024031.

Bogdanov, K. V., Baranov, M. A., Feoktistov, N. A., Kaliya, I. E., Golubev, V. G., Grudinkin, S. A., & Baranov, A. V. (2022). Duo emission of CVD nanodiamonds doped by SiV and GeV color centers: Effects of growth conditions. *Materials, 15*(10), 3589. https://doi.org/10.3390/ma15103589.

Boudou, J. P., Tisler, J., Reuter, R., Thorel, A., Curmi, P. A., Jelezko, F., & Wrachtrup, J. (2013). Fluorescent nanodiamonds derived from HPHT with a size of less than 10 nm. *Diamond and Related Materials, 37*, 80–86. https://doi.org/10.1016/j.diamond.2013.05.006.

Bovenkerk, H. P., Bundy, F. P., Hall, H. T., Strong, H. M., & Wentorf, R. H. (1959). Preparation of diamond. *Nature, 184*(4693), 1094–1098. https://doi.org/10.1038/1841094a0.

Bradac, C., Gaebel, T., Naidoo, N., Sellars, M. J., Twamley, J., Brown, L. J., Barnard, A. S., Plakhotnik, T., Zvyagin, A. V., & Rabeau, J. R. (2010). Observation and control of blinking nitrogen-vacancy centres in discrete nanodiamonds. *Nature Nanotechnology, 5*(5), 345–349. https://doi.org/10.1038/nnano.2010.56.

Bundy, F. P., Hall, H. T., Strong, H. M., & Wentorfjun, R. H. (1955). Man-made diamonds. *Nature, 176*(4471), 51–55. https://doi.org/10.1038/176051a0.

Chen, Y., Li, C., Yang, T., Ekimov, E. A., Bradac, C., Ha, S. T., Toth, M., Aharonovich, I., & Tran, T. T. (2023). Real-time ratiometric optical nanoscale thermometry. *ACS Nano, 17*(3), 2725–2736. https://doi.org/10.1021/acsnano.2c10974.

Crane, M. J., Petrone, A., Beck, R. A., Lim, M. B., Zhou, X., Li, X., Stroud, R. M., & Pauzauskie, P. J. (2019). High-pressure, high-temperature molecular doping of nanodiamond. *Science Advances, 5*(5), eaau6073. https://doi.org/10.1126/sciadv.aau6073.

Danilenko, V. V. (2004). On the history of the discovery of nanodiamond synthesis. *Physics of the Solid State, 46*(4), 595–599. https://doi.org/10.1134/1.1711431.

Davydov, V. A., Agafonov, V., & Khabashesku, V. N. (2016). Comparative study of condensation routes for formation of nano- and microsized carbon forms in hydrocarbon, fluorocarbon, and fluoro-hydrocarbon systems at high pressures and temperatures. *Journal of Physical Chemistry C, 120*(51), 29498–29509. https://doi.org/10.1021/acs.jpcc.6b10805.

Davydov, V. A., Rakhmanina, A. V., Lyapin, S. G., Ilichev, I. D., Boldyrev, K. N., Shiryaev, A. A., & Agafonov, V. N. (2014). Production of nano- and microdiamonds with Si-V and N-V luminescent centers at high pressures in systems based on mixtures of hydrocarbon and fluorocarbon compounds. *JETP Letters, 99*(10), 585–589. https://doi.org/10.1134/s002136401410004x.

Degutis, G., Pobedinskas, P., Turner, S., Lu, Y.-G., Al Riyami, S., Ruttens, B., Yoshitake, T., D'Haen, J., Haenen, K., Verbeeck, J., Hardy, A., & Van Bael, M. K. (2016). CVD diamond growth from nanodiamond seeds buried under a thin chromium layer. *Diamond and Related Materials, 64*, 163–168. https://doi.org/10.1016/j.diamond.2016.02.013.

Ditalia Tchernij, S., Lühmann, T., Herzig, T., Küpper, J., Damin, A., Santonocito, S., Signorile, M., Traina, P., Moreva, E., Celegato, F., Pezzagna, S., Degiovanni, I. P., Olivero, P., Jakšić, M., Meijer, J., Genovese, P. M., & Forneris, J. (2018). Single-photon emitters in lead-implanted single-crystal diamond. *ACS Photonics, 5*(12), 4864–4871. https://doi.org/10.1021/acsphotonics.8b01013.

Feuchtmayr, F., Berghaus, R., Sachero, S., Bayer, G., Lettner, N., Waltrich, R., Maier, P., Agafonov, V., & Kubanek, A. (2023). Enhanced spectral density of a single germanium vacancy center in a nanodiamond by cavity integration. *Applied Physics Letters, 123*(2), 024001. https://doi.org/10.1063/5.0156787.

De Feudis, M., Tallaire, A., Nicolas, L., Brinza, O., Goldner, P., Hétet, G., Bénédic, F., & Achard, J. (2020). Large-scale fabrication of highly emissive nanodiamonds by chemical vapor deposition with controlled doping by SiV and GeV centers from a solid source. *Advanced Materials Interfaces, 7*(2), 1901408. https://doi.org/10.1002/admi.201901408.

Fujisaku, T., Tanabe, R., Onoda, S., Kubota, R., Segawa, T. F., So, F. T. K., Ohshima, T., Hamachi, I., Shirakawa, M., & Igarashi, R. (2019). PH nanosensor using electronic spins in diamond. *ACS Nano, 13*(10), 11726–11732. https://doi.org/10.1021/acsnano.9b05342.

Gottlieb, S., Wöhrl, N., Schulz, S., & Buck, V. (2016). Simultaneous synthesis of nanodiamonds and graphene via plasma enhanced chemical vapor deposition (MW PE-CVD) on copper. *SpringerPlus, 5*(1), 1–16. https://doi.org/10.1186/s40064-016-2201-x.

Greaves, J. S., Scaife, A. M. M., Frayer, D. T., Green, D. A., Mason, B. S., & Smith, A. M. S. (2018). Anomalous microwave emission from spinning nanodiamonds around stars. *Nature Astronomy, 2*(8), 662–667. https://doi.org/10.1038/s41550-018-0495-z.

Hauf, M. V., Grotz, B., Naydenov, B., Dankerl, M., Pezzagna, S., Meijer, J., Jelezko, F., Wrachtrup, J., Stutzmann, M., Reinhard, F., & Garrido, J. A. (2011). Chemical control of the charge state of nitrogen-vacancy centers in diamond. *Physical Review B, 83*(8), 081304. https://doi.org/10.1103/physrevb.83.081304.

Iwasaki, T., Miyamoto, Y., Taniguchi, T., Siyushev, P., Metsch, M. H., Jelezko, F., & Hatano, M. (2017). Tin-vacancy quantum emitters in diamond. *Physical Review Letters, 119*(25), 253601. https://doi.org/10.1103/PhysRevLett.119.253601.

Jantzen, U., Kurz, A. B., Rudnicki, D. S., Schäfermeier, C., Jahnke, K. D., Andersen, U. L., Davydov, V. A., Agafonov, V. N., Kubanek, A., Rogers, L. J., & Jelezko, F. (2016). Nanodiamonds carrying silicon-vacancy quantum emitters with almost lifetime-limited linewidths. *New Journal of Physics, 18*(7), 073036. https://doi.org/10.1088/1367-2630/18/7/073036.

Kageura, T., Kato, K., Yamano, H., Suaebah, E., Kajiya, M., Kawai, S., Inaba, M., Tanii, T., Haruyama, M., Yamada, K., Onoda, S., Kada, W., Hanaizumi, O., Teraji, T., Isoya, J., Kono, S., & Kawarada, H. (2017). Effect of a radical exposure nitridation surface on the charge stability of shallow nitrogen-vacancy centers in diamond. *Applied Physics Express, 10*(5), 055503. https://doi.org/10.7567/apex.10.055503.

Kaviani, M., Deák, P., Aradi, B., Frauenheim, T., Chou, J. P., & Gali, A. (2014). Proper surface termination for luminescent near-surface NV centers in diamond. *Nano Letters, 14*(8), 4772–4777. https://doi.org/10.1021/nl501927y.

Kinzie, C. R., Hee, S. S. Q., Stich, A., Tague, K. A., Mercer, C., Razink, J. J., Kennett, D. J., DeCarli, P. S., Bunch, T. E., Wittke, J. H., Israde-Alcántara, I., Bischoff, J. L., Goodyear, A. C., Tankersley, K. B., Kimbel, D. R., Culleton, B. J., Erlandson, J. M., Stafford, T. W., Kloosterman, J. B., ... Wolbach, W. S. (2014). Nanodiamond-rich layer across three continents consistent with major cosmic impact at 12,800 cal BP. *Journal of Geology, 122*(5), 475–506. https://doi.org/10.1086/677046.

Li, K., Zhou, Y., Rasmita, A., Aharonovich, I., & Gao, W. B. (2016). Nonblinking emitters with nearly lifetime-limited linewidths in CVD nanodiamonds. *Physical Review Applied, 6*(2), 024010. https://doi.org/10.1103/PhysRevApplied.6.024010.

Liang, J., Ender, C. P., Zapata, T., Ermakova, A., Wagner, M., & Weil, T. (2020). Germanium iodide mediated synthesis of nanodiamonds from adamantane "seeds" under moderate high-pressure high-temperature conditions. *Diamond and Related Materials, 108*, 108000. https://doi.org/10.1016/j.diamond.2020.108000.

Lindner, S., Bommer, A., Muzha, A., Krueger, A., Gines, L., Mandal, S., Williams, O., Londero, E., Gali, A., & Becher, C. (2018). Strongly inhomogeneous distribution of spectral properties of silicon-vacancy color centers in nanodiamonds. *New Journal of Physics, 20*(11), 115002. https://doi.org/10.1088/1367-2630/aae93f.

Liu, W., Alam, M. N. A., Liu, Y., Agafonov, V. N., Qi, H., Koynov, K., Davydov, V. A., Uzbekov, R., Kaiser, U., Lasser, T., Jelezko, F., Ermakova, A., & Weil, T. (2022). Silicon-vacancy nanodiamonds as high performance near-infrared emitters for live-cell dual-color imaging and thermometry. *Nano Letters, 22*(7), 2881–2888. https://doi.org/10.1021/acs.nanolett.2c00040.

Mainwood, A. (1999). Point defects in natural and synthetic diamond: What they can tell us about CVD diamond. *physica status solidi (a), 172*(1), 25–35. https://doi.org/10.1002/(SICI)1521-396X(199903)172:1<25::AID-PSSA25>3.0.CO;2-9.

Makino, Y., Yoshikawa, T., Tsurui, A., Liu, M., Yamagishi, G., Nishikawa, M., Mahiko, T., Ohno, M., Ashida, M., & Okuyama, N. (2022). Direct synthesis of group IV-vacancy center-containing nanodiamonds via detonation process using aromatic compound as group IV element source. *Diamond and Related Materials, 130*, 109493. https://doi.org/10.1016/j.diamond.2022.109493.

Mamin, H. J., Kim, M., Sherwood, M. H., Rettner, C. T., Ohno, K., Awschalom, D. D., & Rugar, D. (2013). Nanoscale nuclear magnetic resonance with a nitrogen-vacancy spin sensor. *Science, 339*(6119), 557–560. https://doi.org/10.1126/science.1231540.

Mochalin, V. N., Shenderova, O., Ho, D., & Gogotsi, Y. (2012). The properties and applications of nanodiamonds. *Nature Nanotechnology, 7*(1), 11–23. https://doi.org/10.1038/nnano.2011.209.

Nahra, M., Alshamaa, D., Deturche, R., Davydov, V., Kulikova, L., Agafonov, V., & Couteau, C. (2021). Single germanium vacancy centers in nanodiamonds with bulk-like spectral stability. *AVS Quantum Science, 3*(1), 012001. https://doi.org/10.1116/5.0035937.

Neu, E., Steinmetz, D., Riedrich-Möller, J., Gsell, S., Fischer, M., Schreck, M., & Becher, C. (2011). Single photon emission from silicon-vacancy colour centres in chemical vapour deposition nano-diamonds on iridium. *New Journal of Physics, 13*(2), 025012. https://doi.org/10.1088/1367-2630/13/2/025012.

Nguyen, C. T., Evans, R. E., Sipahigil, A., Bhaskar, M. K., Sukachev, D. D., Agafonov, V. N., Davydov, V. A., Kulikova, L. F., Jelezko, F., & Lukin, M. D. (2018). All-optical nanoscale thermometry with silicon-vacancy centers in diamond. *Applied Physics Letters, 112*(20), 203102. https://doi.org/10.1063/1.5029904.

Plakhotnik, T., Doherty, M. W., Cole, J. H., Chapman, R., & Manson, N. B. (2014). All-optical thermometry and thermal properties of the optically detected spin resonances of the NV- center in nanodiamond. *Nano Letters, 14*(9), 4989–4996. https://doi.org/10.1021/nl501841d.

Pruski, M., Lang, D. P., Hwang, S.-J., Jia, H., & Shinar, J. (1994). Structure of thin diamond films: A H1 and C13 nuclear-magnetic-resonance study. *Physical Review B, 49*(15), 10635–10642. https://doi.org/10.1103/physrevb.49.10635.

Radulaski, M., Zhang, J. L., Tzeng, Y. K., Lagoudakis, K. G., Ishiwata, H., Dory, C., Fischer, K. A., Kelaita, Y. A., Sun, S., Maurer, P. C., Alassaad, K., Ferro, G., Shen, Z. X., Melosh, N. A., Chu, S., & Vučković, J. (2019). Nanodiamond Integration with Photonic Devices. *Laser and Photonics Reviews, 13*(8), 1800316. https://doi.org/10.1002/lpor.201800316.

Reineck, P., Lau, D. W. M., Wilson, E. R., Fox, K., Field, M. R., Deeleepojananan, C., Mochalin, V. N., & Gibson, B. C. (2017). Effect of surface chemistry on the fluorescence of detonation nanodiamonds. *ACS Nano, 11*(11), 10924–10934. https://doi.org/10.1021/acsnano.7b04647.

Rondin, L., Tetienne, J.-P., Hingant, T., Roch, J.-F., Maletinsky, P., & Jacques, V. (2014). Magnetometry with nitrogen-vacancy defects in diamond. *Reports on Progress in Physics, 77*(5), 056503. https://doi.org/10.1088/0034-4885/77/5/056503.

Rose, B. C., Huang, D., Zhang, Z. H., Stevenson, P., Tyryshkin, A. M., Sangtawesin, S., Srinivasan, S., Loudin, L., Markham, M. L., Edmonds, A. M., Twitchen, D. J., Lyon, S. A., & De Leon, N. P. (2018). Observation of an environmentally insensitive solid-state spin defect in diamond. *Science, 361*(6397), 60–63. https://doi.org/10.1126/science.aao0290.

Sahoo, S., Davydov, V. A., Agafonov, V. N., & Bogdanov, S. I. (2023). Hybrid quantum nanophotonic devices with color centers in nanodiamonds [Invited]. *Optical Materials Express, 13*(1), 191–217. https://doi.org/10.1364/OME.471376.

Salz, M., Herrmann, Y., Nadarajah, A., Stahl, A., Hettrich, M., Stacey, A., Prawer, S., Hunger, D., & Schmidt-Kaler, F. (2020). Cryogenic platform for coupling color centers in diamond membranes to a fiber-based microcavity. *Applied Physics B, 126*(8), 131. https://doi.org/10.1007/s00340-020-07478-5.

Schietinger, S., Schröder, T., & Benson, O. (2008). One-by-one coupling of single defect centers in nanodiamonds to high-Q modes of an optical microresonator. *Nano Letters, 8*(11), 3911–3915. https://doi.org/10.1021/nl8023627.

Schröder, T., Fujiwara, M., Noda, T., Zhao, H. Q., Benson, O., & Takeuchi, S. (2012). A nanodiamond-tapered fiber system with high single-mode coupling efficiency. *Optics Express, 20*(10), 10490–10497. https://doi.org/10.1364/OE.20.010490.

Shang, J., Ma, L., Li, J., Ai, W., Yu, T., & Gurzadyan, G. G. (2012). The origin of fluorescence from graphene oxide. *Scientific Reports, 2*, 792. https://doi.org/10.1038/srep00792.

Shenderova, O. A., Shames, A. I., Nunn, N. A., Torelli, M. D., Vlasov, I., & Zaitsev, A. (2019). Review Article: Synthesis, properties, and applications of fluorescent diamond particles. *Journal of Vacuum Science and Technology B: Nanotechnology and Microelectronics, 37*(3), 030802. https://doi.org/10.1116/1.5089898.

Shershulin, V. A., Sedov, V. S., Ermakova, A., Jantzen, U., Rogers, L., Huhlina, A. A., Teverovskaya, E. G., Ralchenko, V. G., Jelezko, F., & Vlasov, I. I. (2015). Size-dependent luminescence of color centers in composite nanodiamonds. *Physica Status Solidi (A) Applications and Materials Science, 212*(11), 2600–2605. https://doi.org/10.1002/pssa.201532204.

Shimazaki, K., Kawaguchi, H., Takashima, H., Segawa, T. F., So, F. T.-K., Terada, D., Onoda, S., Ohshima, T., Shirakawa, M., & Takeuchi, S. (2021). Fabrication of detonation nanodiamonds containing silicon-vacancy color centers by high temperature annealing. *physica status solidi (a), 218*(19), 2100144. https://doi.org/10.1002/pssa.202100144.

Siyushev, P., Metsch, M. H., Ijaz, A., Binder, J. M., Bhaskar, M. K., Sukachev, D. D., Sipahigil, A., Evans, R. E., Nguyen, C. T., Lukin, M. D., Hemmer, P. R., Palyanov, Y. N., Kupriyanov, I. N., Borzdov, Y. M., Rogers, L. J., & Jelezko, F. (2017). Optical and microwave control of germanium-vacancy center spins in diamond. *Physical Review B, 96*(8), 081201. https://doi.org/10.1103/PhysRevB.96.081201.

Smith, B. R., Inglis, D. W., Sandnes, B., Rabeau, J. R., Zvyagin, A. V., Gruber, D., Noble, C. J., Vogel, R., Ösawa, E., & Plakhotnik, T. (2009). Five-nanometer diamond with luminescent nitrogen-vacancy defect centers. *Small, 5*(14), 1649–1653. https://doi.org/10.1002/smll.200801802.

Staudacher, T., Shi, F., Pezzagna, S., Meijer, J., Du, J., Meriles, C. A., Reinhard, F., & Wrachtrup, J. (2013). Nuclear magnetic resonance spectroscopy on a (5-nanometer) 3 sample volume. *Science, 339*(6119), 561–563. https://doi.org/10.1126/science.1231675.

Stehlik, S., Ondic, L., Varga, M., Fait, J., Artemenko, A., Glatzel, T., Kromka, A., & Rezek, B. (2018). Silicon-vacancy centers in ultra-thin nanocrystalline diamond films. *Micromachines, 9*(6), 281. https://doi.org/10.3390/mi9060281.

Stehlik, S., Varga, M., Ledinsky, M., Jirasek, V., Artemenko, A., Kozak, H., Ondic, L., Skakalova, V., Argentero, G., Pennycook, T., Meyer, J. C., Fejfar, A., Kromka, A., & Rezek, B. (2015). Size and purity control of HPHT nanodiamonds down to 1 nm. *Journal of Physical Chemistry C, 119*(49), 27708–27720. https://doi.org/10.1021/acs.jpcc.5b05259.

Tchernij, S. D., Herzig, T., Forneris, J., Küpper, J., Pezzagna, S., Traina, P., Moreva, E., Degiovanni, I. P., Brida, G., Skukan, N., Genovese, M., Jakšić, M., Meijer, J., & Olivero, P. (2017). Single-photon-emitting optical centers in diamond fabricated upon Sn implantation. *ACS Photonics, 4*(10), 2580–2586. https://doi.org/10.1021/acsphotonics.7b00904.

Thiering, G., & Gali, A. (2018). Ab Initio magneto-optical spectrum of group-IV vacancy color centers in diamond. *Physical Review X, 8*(2), 021063. https://doi.org/10.1103/physrevx.8.021063.

Trusheim, M. E., Wan, N. H., Chen, K. C., Ciccarino, C. J., Flick, J., Sundararaman, R., Malladi, G., Bersin, E., Walsh, M., Lienhard, B., Bakhru, H., Narang, P., & Englund, D. (2019). Lead-related quantum emitters in diamond. *Physical Review B, 99*(7), 075430. https://doi.org/10.1103/PhysRevB.99.075430.

Vindolet, B., Adam, M. P., Toraille, L., Chipaux, M., Hilberer, A., Dupuy, G., Razinkovas, L., Alkauskas, A., Thiering, G., Gali, A., De Feudis, M., Ngandeu Ngambou, M. W., Achard, J., Tallaire, A., Schmidt, M., Becher, C., & Roch, J. F. (2022). Optical properties of SiV and GeV color centers in nanodiamonds under hydrostatic pressures up to 180 GPa. *Physical Review B, 106*(21), 214109. https://doi.org/10.1103/PhysRevB.106.214109.

Vlasov, I. I., Shiryaev, A. A., Rendler, T., Steinert, S., Lee, S. Y., Antonov, D., Vörös, M., Jelezko, F., Fisenko, A. V., Semjonova, L. F., Biskupek, J., Kaiser, U., Lebedev, O. I., Sildos, I., Hemmer, P. R., Konov, V. I., Gali, A., & Wrachtrup, J. (2014). Molecular-sized fluorescent nanodiamonds. *Nature Nanotechnology, 9*(1), 54–58. https://doi.org/10.1038/nnano.2013.255.

Westerhausen, M. T., Trycz, A. T., Stewart, C., Nonahal, M., Regan, B., Kianinia, M., & Aharonovich, I. (2020). Controlled doping of GeV and SnV color centers in diamond using chemical vapor deposition. *ACS Applied Materials and Interfaces, 12*(26), 29700–29705. https://doi.org/10.1021/acsami.0c07242.

Wolters, J., Schell, A. W., Kewes, G., Nüsse, N., Schoengen, M., Döscher, H., Hannappel, T., Löchel, B., & Barth, M. (2010). Enhancement of the zero phonon line emission from a single nitrogen vacancy center in a nanodiamond via coupling to a photonic crystal cavity. *Applied Physics Letters, 97*(14), 141108. https://doi.org/10.1063/1.3499300.

Wu, Y., Ermakova, A., Liu, W., Pramanik, G., Vu, T. M., Kurz, A., McGuinness, L., Naydenov, B., Hafner, S., Reuter, R., Wrachtrup, J., Isoya, J., Förtsch, C., Barth, H., Simmet, T., Jelezko, F., & Weil, T. (2015). Programmable biopolymers for advancing biomedical applications of fluorescent nanodiamonds. *Advanced Functional Materials, 25*(42), 6576–6585. https://doi.org/10.1002/adfm.201502704.

Zaitsev, A. M. (2001). *Optical Properties of Diamond: A Data Handbook*, *2001*. Springer Link.